IJMMM International Journal of Minerals, Metallurgy and Materials 矿物冶金与材料学报（英文版）

A review on the critical challenges and progress of SiO_x-based anodes for lithium-ion batteries

Nana Yao, Yu Zhang, Xianhui Rao, Zhao Yang, Kun Zheng, Konrad wierczek, and Hailei Zhao

Cite this article as:
Nana Yao, Yu Zhang, Xianhui Rao, Zhao Yang, Kun Zheng, Konrad wierczek, and Hailei Zhao, A review on the critical challenges and progress of SiO_x-based anodes for lithium-ion batteries, *Int. J. Miner. Metall. Mater.*, 29(2022), No. 4, pp. 876-895. https://doi.org/10.1007/s12613-022-2422-7

View the article online at SpringerLink or IJMMM Webpage.

International Journal of Minerals, Metallurgy and Materials
Volume 29, Number 4, April 2022, Page 876
https://doi.org/10.1007/s12613-022-2422-7

Invited Review

A review on the critical challenges and progress of SiO_x-based anodes for lithium-ion batteries

Nana Yao[1),*], *Yu Zhang*[1),*], *Xianhui Rao*[1),*], *Zhao Yang*[1)], *Kun Zheng*[2)], *Konrad Świerczek*[2)], *and Hailei Zhao*[1,3),✉]

1) School of Materials Science and Engineering, University of Science and Technology Beijing, Beijing 100083, China
2) Faculty of Energy and Fuels, AGH University of Science and Technology, al. A. Mickiewicza 30, Krakow, 30-059, Poland
3) Beijing Key Lab of New Energy Materials and Technology, Beijing 100083, China
(Received: 9 October 2021; revised: 8 January 2022; accepted: 17 January 2022)

Abstract: With the advantages of abundant resources, high specific capacity, and relatively stable cycling performance, silicon suboxides (SiO_x, $x < 2$) have been recently suggested as promising anodes for next-generation lithium-ion batteries (LIBs). SiO_x exhibits superior storage capability because of the presence of silicon and smaller volume change upon charge/discharge than Si owing to the buffering effect of the initial lithiation products of inert lithium oxide and lithium silicates, enabling a stable cycle life of electrodes. However, significant improvements, such as overcoming issues related to volume changes in cycling and initial irreversible capacity loss and enhancing the ionic and electronic charge transport in poorly conducting SiO_x electrodes, are still needed to achieve the satisfactory performance required for commercial applications. This review summarizes recent progress on the cycling performance and initial coulombic efficiency of SiO_x. Advances in the design of particle morphology and composite composition, prelithiation and prereduction methods, and usage of electrolyte additives and optimized electrode binders are discussed. Perspectives on the promising research directions that might lead to further improvement of the electrochemical properties of SiO_x-based anodes are noted. This paper can serve as a basis for the research and development of high-energy-density LIBs.

Keywords: silicon suboxides; preparation; structural optimization; anode; lithium-ion batteries

1. Introduction

Non-renewable resources, such as coal, oil, and natural gas, are still used and consumed worldwide in large quantities, causing a rapid drop in their reserves and leading to greenhouse effect intensification, widespread water and air pollution, and other negative phenomena. To alleviate these issues, electric vehicles have been vigorously promoted worldwide in recent years. Lithium-ion batteries (LIBs) have dominated the power source market of electric vehicles because of their several advantages, such as high energy density, high working voltage, long cycling life, and low self-discharge [1]. However, the energy density of current LIBs cannot meet the ever-increasing mileage need of electric transportation, which limits their wide deployment [2]. Thus, exploring new electrode materials with high energy density has become the top priority in the R&D of LIBs.

Anodes exert a decisive influence on the electrochemical performance of LIBs. At present, graphite-based anodes are widely utilized in commercial LIBs, and the specific capacity of such anodes has already reached 340–365 $mAh \cdot g^{-1}$, which is close to the theoretical value [3]. With the growing demand for high-energy-density LIBs, the development of new anodes with high specific capacities is imperative. Instead of intercalation-class materials, either conversion reaction or alloying-type compounds have been proposed and widely studied [4–5]. Silicon is a promising anode because of its high theoretical specific capacity (4200 $mAh \cdot g^{-1}$), suitable operating voltage, abundant natural resources, and associated low costs [6]. However, the mechanical instability of Si-based electrodes due to large volume changes during lithiation/delithiation, typical for the alloying-type reaction [7–8], causes particle cracking and pulverization, resulting in poor cycling performance of Si-based anodes [9–10]. Many approaches, including the design of nanostructure-scale particles [11–12], formation of Si-containing composites [13–15], and optimization of electrode film structure [16–17], have been proposed to solve this problem. Despite numerous reports on the improvement of the electrochemical properties of Si anodes, less commercial breakthrough in high-Si-content electrodes has been achieved. In modifying silicon anodes, researchers found that SiO_x-type ($0 < x < 2$) nonstoichiometric oxides exhibit much better cycling stability than pure Si because of the reduced volume expansion in

*These authors contributed equally to this work.
✉ Corresponding author: Hailei Zhao E-mail: hlzhao@ustb.edu.cn

reaction with lithium. Therefore, SiO_x has become an excellent candidate anode for high-energy-density LIBs in recent years.

The fundamental difference regarding the charge/discharge mechanism of SiO_x with Si anodes stems from the irreversible formation of inert components (Li_2O, various lithium silicates) during the first lithiation, whose presence can dilute the volume changes of active particles and thus reduce the mechanical stresses of electrodes, ensuring a relatively stable cycling performance of SiO_x-based electrodes [18–20]. Nevertheless, the cycling stability of SiO_x electrodes is far from the requirement in practical applications. Irreversibly formed inert components contribute a large part of irreversible capacity, causing a much lower initial coulombic efficiency (ICE). In addition, the poor ionic and electronic conductivity of SiO_x limit the electrode reaction kinetics and thus the rate performance.

Facing the challenges of SiO_x application, various strategies, including particle morphology design [21–22], combination with conductive second phase [23–24], usage of proper binders [25– 26], and advanced additives [27], have been proposed to address the issues mentioned above. In this review, we first introduce the structural characteristics of SiO_x and the electrochemical reaction mechanism with lithium. Then, we summarize the progress in the fabrication of SiO_x materials in recent years. Finally, we discuss the improvement and advancement of the electrochemical performance of SiO_x anodes, with an outlook given regarding the possible further development of such electrodes.

2. Oxygen content and atomic-scale structure of SiO_x

Despite many reports, the structural model of SiO_x remains controversial. Initially, in the 1970s, two main structural models were reported for the amorphous SiO_x, namely, Random-bonding (RB) [28–29] and random-mixture (RM) [30]. The RB model infers that the structure of SiO_x consists of a continuous random distribution formed by Si–Si and Si–O bonds, which run through the entire structural network. By contrast, the RM model proposes that SiO_x is generally a dual-phase material composed of regions comprising amorphous Si and crystalline SiO_2, with a particle size of both fractions being less than 1 nm. This corresponds to the composite-type material at nanoscale, but with respective regions being extremely small, i.e., technically not forming separate phases. Both models have been reported with supporting results [31–32].

Based on the two models mentioned above, Hohl *et al.* [33] proposed the interface cluster mixture (ICM) model (Fig. 1(a)), which assumes that SiO_x is composed of SiO_2 clusters (light gray) and Si clusters (black), as well as the ultrathin suboxide (in terms of local oxygen content) interface (gray), forming a matrix-like structure. Compared with previous models, the ICM model is more consistent with the reported electrochemical performance of SiO_x in elucidating the electrochemical reaction mechanism with lithium [34]. Using angstrom-beam electron diffraction combined with synchrotron X-ray scattering and computer simulations, Hirata *et al.* [35] studied the SiO_x structure. Their experimental results uncovered the non-uniform distribution of Si and O at the atomic scale and verified the heterostructural model of Si clusters mixing with amorphous SiO_2 (Fig. 1(b)). The two regions are connected by various suboxide-type interfacial regions with generally tetrahedral coordination.

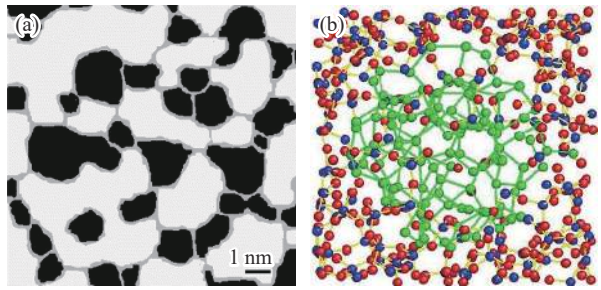

Fig. 1. Schematic of a-SiO structure: (a) the interface clusters mixture model (the gray, light gray, and black regions represent sub-oxidic interface, SiO_2 clusters, and Si clusters, respectively); (b) the reconstructed heterostructure model (the blue, red, and green spheres represent Si and O in amorphous SiO_2 and Si in Si clusters, respectively). (a) Reprinted from *J. Non Cryst. Solids*, 320, A. Hohl, T. Wieder, P.A. van Aken, T.E. Weirich, G. Denninger, M. Vidal, S. Oswald, C. Deneke, J. Mayer, and H. Fuess, An interface clusters mixture model for the structure of amorphous silicon monoxide (SiO), 255-280, Copyright 2003, with permission from Elsevier; (b) reprinted by permission from Springer Nature: *Nat. Commun.*, Atomic-scale disproportionation in amorphous silicon monoxide, A. Hirata, S. Kohara, T. Asada, M. Arao, C. Yogi, H. Imai, Y.W. Tan, T. Fujita, and M.W. Chen, Copyright 2016.

With the intrinsic limitations of X-ray diffraction and other methods used for structural characterization, a complete picture showing the actual atomic-scale structure of SiO_x remains challenging to provide.

3. Lithiation/delithiation mechanism of SiO_x

Many efforts have been exerted to elucidate the lithiation process of SiO_x. The reactivity of SiO_x depends on stoichiometry and crystallinity. Crystalline SiO_2 cannot react with lithium, whereas nanosized SiO_2 [36–38] and amorphous SiO_2 domains presenting in the SiO [39–42] can electrochemically react with lithium to form lithium silicates and Li_2O. Yamamura *et al.* [43] reported that even amorphous SiO_2 can react with lithium because of the presence of distorted SiO_4 tetrahedrons. Nevertheless, the stoichiometric SiO_2 is generally considered to be less active, and the nonstoichiometric SiO_x with $x<2$ is active toward lithium storage.

The lithiation/delithiation mechanism of SiO_x material is still not very clear, especially regarding the nature and reversibility of the electrochemical processes for the formed Li_x-Si alloy and lithium silicates during the first lithiation. Nevertheless, Si, lithium silicates, and Li_2O are generally believed

to form first during the first lithiation of SiO_x, and then Si is further lithiated (alloying-type of reaction) to form Li_xSi alloy, typically up to x = 3.75 [20,34,39,44–52]. Formation of Li_xSi alloy is reversible, occurs at advantageous low potentials vs. Li electrode, and provides the main part of the reversible capacity. By contrast, the formed lithium silicates (e.g., Li_4SiO_4, $Li_6Si_2O_7$, Li_2SiO_3) during the first lithiation are generally described as irreversible phases. The exception is Li_2SiO_5, in which the lithium is considered deliverable but does not contribute a substantial reversible capacity. In addition, the formation of Li_2O is most possibly irreversible [18,39,44–45]. Interestingly, numerous reports have proven that the electrochemically inactive lithium silicates and Li_2O can provide crucial advantages for the electrode reaction, not only relieving the volume change of the SiO_x-based anodes on lithiation/delithiation but also enhancing the diffusion of Li^+ in the electrode, which contribute much to the improved cycling stability and rate performance [18,20,39,47–48]. In addition, the amount of the formed electrochemically inactive products is strongly dependent on the electrode charge/discharge current density. More irreversible products will be generated at low C-rates with sufficient Li^+ provided, whereas the amount of the electrochemically inactive phases decreases faster at high C-rates [53].

For the initial lithiation products of SiO_x, Kim *et al*. [34] proposed the formation of $Li_{15}Si_4$ for Si clusters, $Li_2O/Li_{15}Si_4$ for SiO interphase, and $Li_4SiO_4/Li_{15}Si_4$ for silicon oxide part based on the RM structure model. As a result, 4.2 mol of Li are supposed to be stored by 1 mol SiO. However, subsequent investigation shows that various lithium silicates can form in the initial lithiation, and some of them can be reversible. The lithiation/delithiation mechanism of SiO_x powders prepared through high-energy mechanical milling (HEMM) was investigated using ex situ high-resolution transmission electron microscopy (HRTEM) [54]. In the first lithiation, unreacted Si and $Li_2Si_2O_5$ phases appeared first when the potential was lowered to 0.27 V (Fig. 2(a)). Then, Li_4SiO_4 formed subsequently at 0.24 V (Fig. 2(b)). Finally, the $Li_{15}Si_4$ phase was obtained when the potential reached 0 V (Fig. 2(c)). When Li^+ was extracted, decomposition of $Li_{15}Si_4$ occurred first at 0.34 V (Fig. 2(d)). Then, $Li_2Si_2O_5$ reacted with Si to generate SiO_2 ($Li_2Si_2O_5 + (1/2)Si \rightarrow (5/2)SiO_2 + 2Li^+ + 2e^-$) at 0.39 V (Fig. 2(e)). This product could also be detected after 10 cycles, suggesting that the formation of $Li_2Si_2O_5$ is

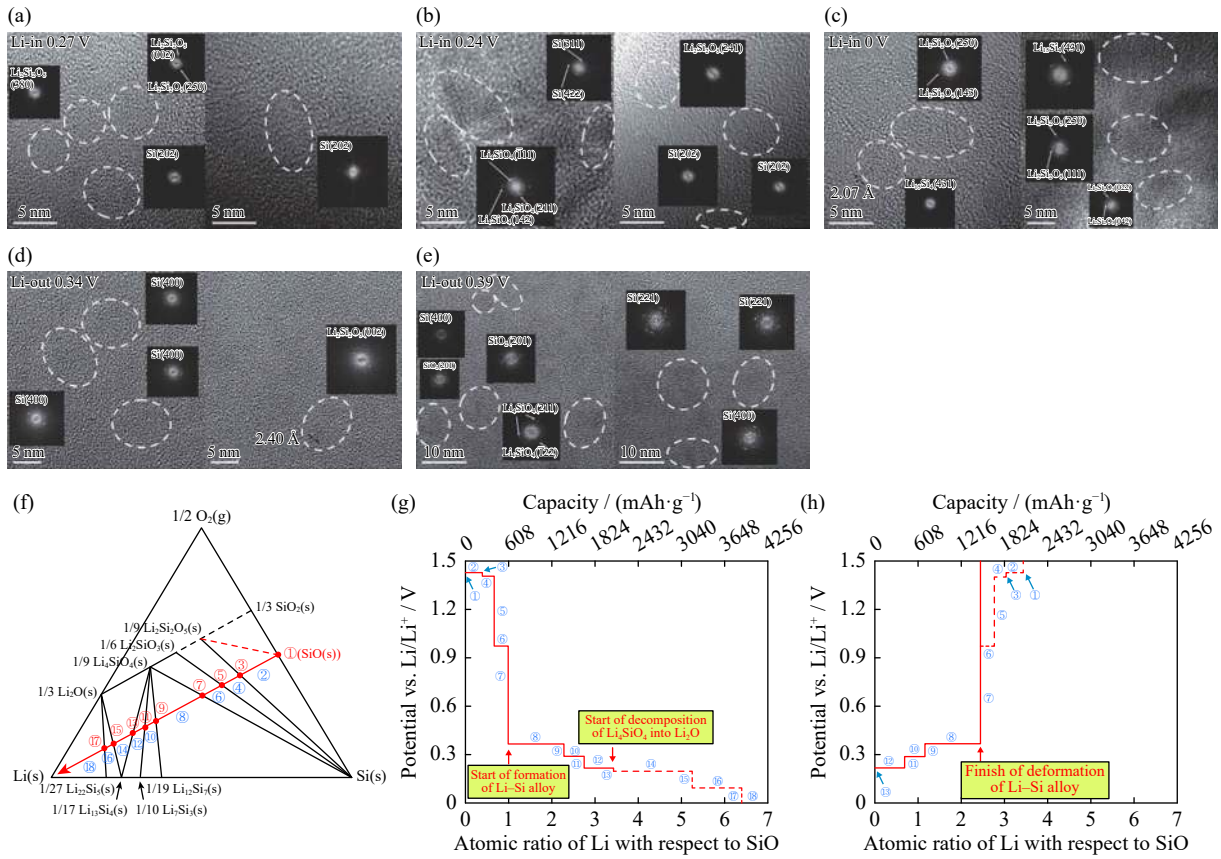

Fig. 2. Ex situ HRTEM images when SiO was discharged to (a) 0.27 V, (b) 0.24 V, and (c) 0.0 V, and charged to (d) 0.34 V and (e) 0.39 V; (f) transition between formed phases during Li insertion for SiO negative electrode at 298 K, data shown in the ternary Li-Si-O phase diagram; changes in the equilibrium SiO electrode potential at 298 K during (g) Li insertion and (h) Li removal after the formation of $Li_{13}Si_4$. (a–e) Reprinted with permission of Royal Society of Chemistry, from Quartz (SiO_2): A new energy storage anode material for Li-ion batteries, W.S. Chang, C.M. Park, J.H. Kim, Y.U. Kim, G. Jeong, and H.J. Sohn, 5, 5, Copyright 2012, permission conveyed through Copyright Clearance Center, Inc.; (f–h) reprinted from *J. Power Sources*, 329, K. Yasuda, Y. Kashitani, S. Kizaki, K. Takeshita, T. Fujita, and S. Shimosaki, Thermodynamic analysis and effect of crystallinity for silicon monoxide negative electrode for lithium ion batteries, 462-472, Copyright 2016, with permission from Elsevier.

reversible.

The behavior of SiO_x suboxides with highly differing x values (x = 0.17, 0.51, 1.02, and 1.34) in the charge and discharge processes was investigated through X-ray photoelectron spectroscopy [19]. Fully lithiated $Li_{4.4}Si$, Li_2O, Li_4SiO_4, and Li_2SiO_3 form after the first discharge. Aside from the Li_2O and lithium silicates, a portion of Li_xSi ($x < 2$) could not be fully delithiated and remained after the first charge process, which also contributes to the irreversible capacity loss of SiO_x on cycling. In addition, Li_2SiO_3 might be a more stable irreversible phase than Li_4SiO_4 when $SiO_{1.34}$ was utilized, whereas Li_4SiO_4 was more stable when lower oxygen contents $SiO_{0.17}$, $SiO_{0.51}$, and $SiO_{1.02}$ were first lithiated.

Yasuda *et al*. [55] explored the lithiation mechanism of SiO by thermodynamic analysis and electrochemical experiments. The results are summarized in Fig. 2(f)–(h). (1) Lithium silicates ($Li_2Si_2O_5$, Li_2SiO_3, and Li_4SiO_4) should appear together with the formation of Si (from point 1 to point 7 in the graphs) up to the discharge capacity of 608 $mAh \cdot g^{-1}$, which is consistent with 600 $mAh \cdot g^{-1}$ capacity in the 0.35–0.5 V range from the lithiation curve of the amorphous SiO in practical experiments; (2) the formed Si reacts with Li to form Li-Si alloys ($Li_{12}Si_7$, Li_7Si_3, and $Li_{13}Si_4$) that are in equilibrium with Li_4SiO_4 (from point 7 to 13), corresponding to a total discharge capacity of 2090 $mAh \cdot g^{-1}$, which does not match the measured capacity of 2600 $mAh \cdot g^{-1}$ in the 0.05–0.35 V range, even if the capacities of the conductive additive and binder are deducted. This result suggests the partial decomposition of already formed lithium silicates into Li_2O, which occurs with the concomitant release of Si. The latter can contribute extra capacity with respect to the theoretical prediction; (3) Upon further lithiation, the Li_4SiO_4 phase is decomposed to form Li_2O and $Li_{13}Si_4$; (4) Further Li^+ insertion produces $Li_{22}Si_5$ from $Li_{13}Si_4$ (from point 15 to 17), with a total discharge capacity of 2891 $mAh \cdot g^{-1}$; (5) finally, metallic Li is deposited at the lowest voltages, close to 0.0 V (after point 18) [55].

Molecular dynamic simulations were adopted to investigate the lithiation mechanism of SiO. Results indicated that Li_xSiO can theoretically store up to x = 5.22 of lithium, corresponding to a higher capacity of 3172 $mAh \cdot g^{-1}$, when Li_2O becomes dominant over Li-silicates. However, owing to large activation barriers that should be overcome to decompose the SiO_4 tetrahedral units in Li-silicates, the evolution of $Li_2Si_2O_5$, $Li_6Si_2O_7$, and Li_4SiO_4 into Li_2O is kinetically impossible under electrochemical conditions. Only $Li_{4.39}SiO$ composition (i.e., average x = 4.39) can be achieved in practical experiments. They suggested that Li-silicates are dominant over Li_2O as the formed irreversible subphases. The kinetically controlled transformation of Li-silicates into Li_2O in the matrix should lead to great improvements in the reversible capacity and rate capability of SiO [20].

Although extensive investigations have been carried out on the lithiation/delithiation mechanism of SiO_x, some divergence still exists, especially on the issues of the final lithiation products and the reversibility of some of these lithium silicates. Nonetheless, the viewpoints that $Li_{15}Si_4$ is the final lithium-silicon alloying product and that Li_4SiO_4 is an irreversible lithiation product are widely accepted [34,43,45,55]. Apparently, the lithiation/delithiation mechanisms of SiO_x must be understood to improve the ICE and enhance the electrochemical performance effectively.

4. Synthesis methods of electrochemically-active SiO_x

Many efforts have been devoted to the synthesis of SiO_x anodes because it is not a naturally stable phase structure. The successful methods reported can be generally grouped into three approaches: (1) thermal evaporation [18–19, 56–57], (2) wet-chemistry [58–61], and (3) HEMM [48,52,62], which are illustrated in Fig. 3.

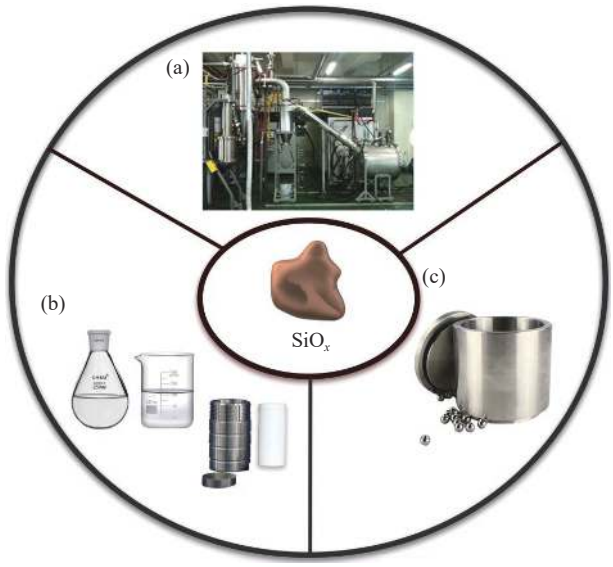

Fig. 3. Schematic of major preparation methods of SiO_x: (a) thermal evaporation [63]; (b) wet-chemistry; (c) HEMM. (a) Reprinted from *Electrochim. Acta*, 148, S.S. Suh, W.Y. Yoon, D.H. Kim, S.U. Kwon, J.H. Kim, Y.U. Kim, C.U. Jeong, Y.Y. Chan, S.H. Kang, and J.K. Lee, Electrochemical behavior of SiO_x anodes with variation of oxygen ratio for Li-ion batteries, 111-117, Copyright 2014, with permission from Elsevier.

4.1. Thermal evaporation methods

The widely adopted method for SiO_x synthesis on an industrial scale is thermal evaporation, in which SiO_x powder is produced by sublimating and condensing SiO_2 and Si under high temperatures [56,64–66]. Moreover, SiO_x materials with different silicon/oxygen ratios can be prepared by adjusting the ratio of raw materials and process conditions [67]. Shin-Etsu Chemical Co., Ltd. of Japan, Osaka Titanium Technologies Co., Ltd. of Japan, and Samsung SDI Co., Ltd. of South Korea used this method to produce SiO_x powders as an anode component for LIBs on a commercial scale.

In addition, other physical and chemical techniques are explored to fabricate SiO_x powders or films include vacuum electron beam evaporation [19], plasma spray physical vapor

deposition [57,63], and infrared ray nanosecond laser ablation [68]. SiO_x with different silicon/oxygen ratios (x value) can be obtained by controlling the processing parameters. As an example, Takezawa *et al*. [19] used vacuum electron beam evaporation to deposit amorphous SiO_x films on copper substrates through a reaction between evaporative Si and oxygen, and the x value could be controlled by oxygen flow rate. Therefore, SiO_x films with different silicon/oxygen ratios (x = 0.17, 0.51, 1.02, and 1.34) could be prepared, which enabled the study of the influence of total oxygen content on the electrochemical properties of SiO_x.

Considering industrial applications, thermal evaporation methods exhibit important advantages related to the control of the total oxygen content in the material. However, their usage for the commercial-scale synthesis of LIBs remains to have substantial issues, including large equipment investment, high energy consumption, and low productivity, resulting in the high cost of SiO_x products.

4.2. Wet-chemistry routes

Wet-chemistry synthesis routes are widely used in the preparation of various type powders because of the advantages of the homogenous, atomic-scale mixing of the elements ensured at the initial stages of the procedure, the controllable particle size and morphology of the product, as well as low-energy consumption and associated low costs [58,69–70].

The sol–gel methods are reported for the preparation of SiO_x materials [58–61]. The reaction conditions, including starting chemicals, surfactants, catalysts, hydrolysis time, drying, and reagent ratio, must be thoughtfully adjusted to obtain the desired phase composition, structure, and morphology of the product. Liu *et al*. [58] used vinyltriethoxysilane (VTES) as the silicon source for the preparation of SiO_x powders. Under Stöber reaction conditions, VTES was hydrolyzed and condensed to produce organosilicate, which was subsequently processed to generate SiO_x microspheres. In addition, tetraethoxysilane (TEOS) [21,60,71–75] and tetramethoxysilane [76–77] are frequently used as silicon sources. Various material structures were prepared by combining the template with a hydrothermal method [78–82]. With CTAB-assisted resorcinol self-assembly as a template, Ren and Li [81] prepared rod-like SiO_x@C composite with individual rod containing numerous interconnected nanospheres by using a hydrothermal method with a post pyrolysis process. The network-structured SiO_x/MWCNT/N-doped C composite was fabricated as LIB anode through precipitation and pyrolysis by using triethoxyethylsilane ($(C_2H_5O)_3SiC_2H_5$) as the silicon source [83].

Our group worked in this direction for more than ten years. Amorphous SiO_x powders with different particle sizes were synthesized as anode materials for LIBs from TEOS via sol–gel and hydrothermal methods [71–73,84]. With CTAB and PVP self-assembled template, the mesoporous SiO_x/C composite with an arrayed molecular-sieve architecture was prepared from TEOS and sucrose via a hydrothermal route [82]. SiO_x–C dual-phase glass was fabricated via a sol–gel method combined with calcination to increase the tapping density [71]. The phase composition and the oxygen nonstoichiometry of SiO_x can be controlled by optimizing the processing parameters. High Si content with a low x value of SiO_x can deliver a high specific capacity, which can be achieved by preparing a highly porous SiO_x-based material with a high specific surface area to realize sufficient reduction via a wet-chemistry route [74,85].

The wet-chemistry route for SiO_x synthesis has advantages in the chemical homogeneity and controllable morphology of target materials, as well as in capital investment reduction, which ensures a good demonstration of electrochemical performance and is conducive to the deployment of SiO_x anodes in the practical battery industry.

4.3. High energy mechanical milling

Compared with the traditional energy-consuming preparation processes, HEMM is simple in operation. The SiO_x powders can be synthesized using HEMM from Si and SiO_2, and the particle size of SiO_x can be controlled by adjusting the time of ball milling [86]. As reported, Si/O_2 can also be used as raw materials to synthesize SiO_x, and the x value in SiO_x can be tailored by tuning the exposure time of pure silicon powder to air [62,86–87]. For example, Cao *et al.* [62] prepared an amorphous SiO_x anode with oxygen content between $0 \le x \le 0.37$ through HEMM of Si powder in the air. The amorphous SiO_x has a particle structure of the nano-Si core surrounding with amorphous SiO_x.

HEMM can reduce the activation energy of a reaction between the starting chemicals and realize the synthesis of materials at low temperatures. In general, the particle size decreases with ball milling time extension, but may cause secondary agglomeration and produce impurities originating from the milling chamber and balls. Thus, appropriate ball-milling conditions must be controlled accurately to obtain the desired oxygen content and particle size of the synthesized SiO_x.

5. Fundamental challenges and solutions to overcome limitations of SiO_x anodes

As mentioned above, the inert buffer matrix composed of lithium silicates and Li_2O formed in the first lithiation of SiO_x anodes helps mitigate volume changes in reversible electrochemical processes and therefore improves the cycle stability of silicon suboxides as compared with pure Si. However, SiO_x anodes still have considerable volume changes (~200%) upon lithiation/delithiation processes, which has the potential to destroy the electrode structure and cause a rapid capacity decay. Moreover, the electrochemically inactive lithium silicates and Li_2O formed in the first lithiation result in a low ICE, and the low intrinsic electrical conductivity limits the rate performance of SiO_x electrodes [50]. These disadvantageous effects are associated with the following major challenges: (1) material pulverization effect on cycling, (2) unstable solid-electrolyte interphase (SEI) film,

(3) low ICE, and (4) electrode failure by cracking.

5.1. Morphology design for mitigating the pulverization of SiO_x on cycling

The capacity of pure silicon suboxide electrodes usually degrades rapidly with cycling because of the particle pulverization caused by the mechanical stresses related to the volume changes. One of the effective approaches to address this issue is to build special particle structures, such as core-shell, yolk-shell, porous, and hollow structures, constructing buffer layers or providing sufficient space to accommodate the volume change.

For the core-shell structure, a layer of conductive material, such as carbon or metal oxide, can be coated on the surface of SiO_x [72,88–94]. This type of structure can effectively limit the volume expansion and improve the electronic conduction of SiO_x. For example, our group synthesized a core-shell structure composed of SiO_x nanoparticles coated with a thin carbon layer through a simple and efficient wet-chemical synthesis route, which provides a stable reversible capacity of 820 $mAh \cdot g^{-1}$ after 100 cycles [72]. In addition, the dual-shell coating structural composites can further inhibit the structural damage caused by internal stress. Xiao *et al*. [89] synthesized SiO_x@TiO_2@C composite, and the introduced TiO_2 layer with a high-crystallinity anatase phase can improve the overall interface stability of the electrode. The volume change of the electrode is effectively buffered, the discharge capacity retention is 89.5% after 800 cycles at a current density of 1.0 $A \cdot g^{-1}$.

Different morphology designs also aim to create a free space that can buffer the volume changes of SiO_x material [70,74,82,85,95–98]. As shown in Fig. 4(a)–(f), porous, hollow, and yolk-shell structures can provide abundant free space. Lee and Park [96] introduced a simple method to synthesize a 3D porous silicon monoxide anode through wet-chemical etching using bulk silica powder as the raw material (Fig. 4(a) and (b)). The porous structure can effectively buffer the volume expansion of SiO_x and promote a stable cycling performance. However, its high specific surface area causes excessive SEI generation, resulting in a low ICE of 60%. To address this issue, the author subsequently coated the surface with a carbon layer and increased the ICE to 76%. The yolk-shell and hollow structures were prepared using chemical etching, respectively (Fig. 4(c)–(f)) [98–99]. These structures enable SiO_x material to expand freely into the interior on lithiation, whereas the outer carbon-shell coating

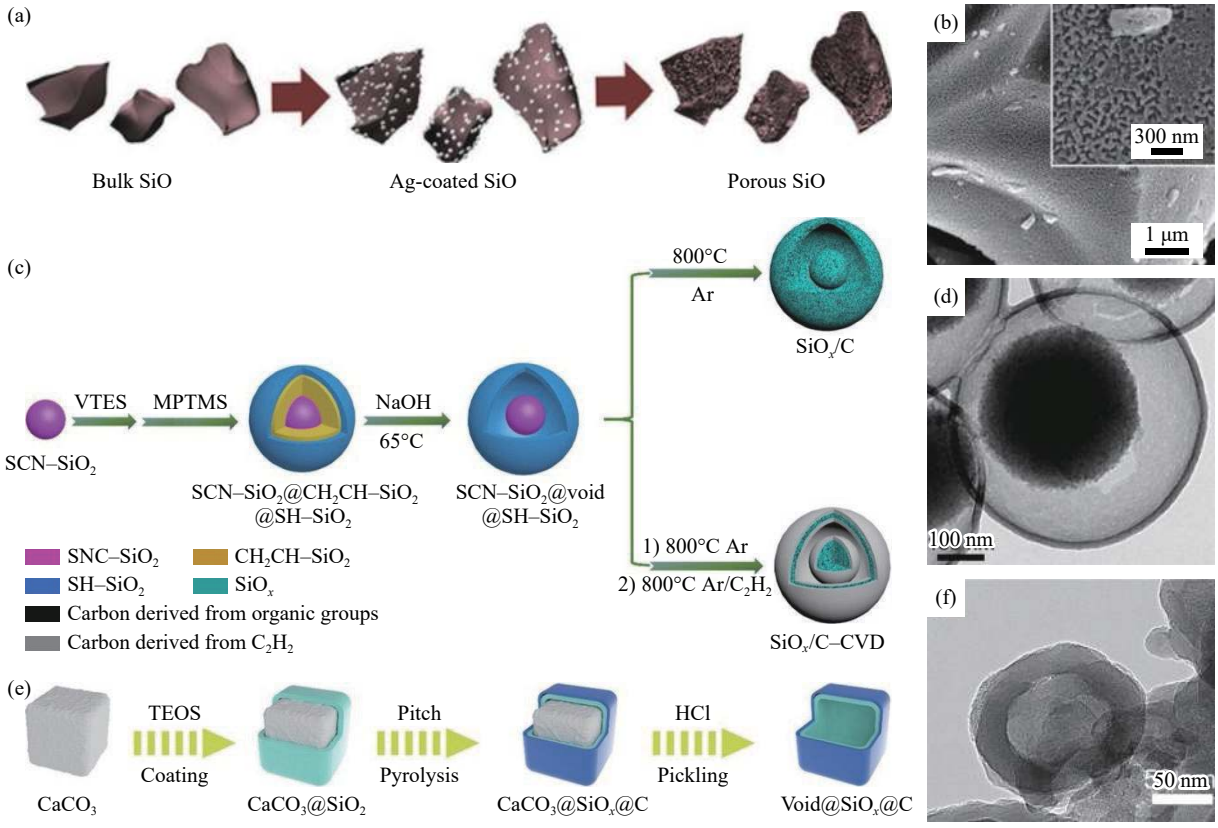

Fig. 4. (a) Schematic showing the synthesis route of porous SiO using Ag catalytic etching; (b) SEM micrograph of the obtained porous SiO_x; (c) preparation of yolk-shell SiO_x/C and SiO_x/C microspheres; (d) TEM image of yolk-shell SiO_x/C; (e) schematic of synthesis process for void@SiO_x@C; (f) SEM image of hollow void@SiO_x@C. (a, b) Reprinted from *Nano Energy*, 2, J.I. Lee and S. Park, High-performance porous silicon monoxide anodes synthesized via metal-assisted chemical etching, 146-152, Copyright 2013, with permission from Elsevier; (c, d) reprinted from *Energy Storage Mater*., 19, Z.H. Liu, Y.L. Zhao, R.H. He, W. Luo, J.S. Meng, Q. Yu, D.Y. Zhao, L. Zhou, and L.Q. Mai, Yolk@shell SiO_x/C microspheres with semi-graphitic carbon coating on the exterior and interior surfaces for durable lithium storage, 299-305, Copyright 2019, with permission from Elsevier; (e, f) D.L. He, P. Li, W. Wang, Q. Wan, J. Zhang, K. Xi, X.M. Ma, Z.W. Liu, L. Zhang, and X.H. Qu, *Small*, 16, art. No. 1905736 (2020) [99]. Copyright Wiley-VCH Verlag GmbH & Co. KGaA. Reproduced with permission.

maintains the integrity of the whole particle structure, which is beneficial to the interface stability, thus promoting the steady growth of the SEI film. The yolk-shell structured SiO_x/C material shows a good cycle performance of 972 $mAh·g^{-1}$ after 500 cycles at 500 $mA·g^{-1}$ [98]. Our team prepared a dandelion-like highly porous SiO_x particle coated with a conformal carbon layer, in which the abundant mesopores effectively accommodate the volume variation of the particles upon lithiation, thereby endowing the material with an excellent cycle stability of 88.6% capacity retention at 2 $A·g^{-1}$ after 1000 cycles [74].

5.2. SiO_x-based composite anode materials

Another effective way to resolve the particle pulverization is to combine SiO_x with a second phase to form multiphase architecture (carbon, metal, metal oxide, etc.). The second phase can buffer the volume change caused by SiO_x lithiation, prevent the aggregation of SiO_x particles, and/or construct a conducting network between the particles to improve the cycling performance of the electrode.

5.2.1. SiO_x/C composites

Combining SiO_x with carbon materials is a common, simple, economical, and overall promising approach to improve the performance of SiO_x anodes. Carbon materials can efficiently improve the conductivity and thereby promote the reaction kinetics occurring at the electrodes. Furthermore, carbon materials can properly buffer the volume changes of SiO_x during cycling and thus enhance electrode stability [51]. Several methods can be employed to synthesize SiO_x/C composites, but the electrochemical properties of the prepared composites differ greatly. A general overview of the recently published results is shown in Table 1.

As observed from Table 1, the carbon materials applied to form composites with SiO_x mainly include graphite, amorphous carbon, graphene, and carbon-based nanomaterials. Graphite is known for its good electrical conductivity, which can enhance the electrode reaction kinetics of SiO_x. SiO_x/graphite composites can be prepared by direct mixing or by coating the surface of SiO_x with graphitized carbon [103,106,116].

An amorphous carbon layer can be formed by mixing SiO_x with organic materials and calcining at high temperatures. The formed carbon shell layer effectively improves the conductivity of SiO_x-based composites and buffers the volume changes of SiO_x during lithiation/delithiation. Compared with a direct mixing method, adding carbon source in a sol–gel process allows to realize a uniform dispersion of carbon source with silicon source in controlled hydrolysis [69,71,84,104,117]. Uniformly dispersed SiO_x/C composites can also be synthesized using a hydrothermal method [72,108,118]. As a representative sample, SiO_x/C composite spheres prepared from the mixture of polydimethylsiloxane

Table 1. Comparison of electrochemical performance of SiO_x–C composite electrodes.

Anode material	Carbon source	Carbon content / wt%	Initial discharge capacity ($mAh·g^{-1}$)/ Charge capacity ($mAh·g^{-1}$)/Coulombic efficiency (%)/Current density ($mA·g^{-1}$)	Stable capacity ($mAh·g^{-1}$) / Number of cycles	Year	Ref.
SiO_x/C	Citric acid	1	1995/1297/65/100	844/200	2017	[100]
Si−SiO_x−C	Citric acid	11	1948/1562/80/100	1373/100	2017	[101]
Si/SiO_x@C	Sucrose	63	1619/1214/75/100	1095/100	2018	[102]
SiO_x/C	RF	40	1460/965/66/100	854/150	2018	[58]
SiO_x/rGO	rGO	—	3765/2564/68/100	580/200	2018	[78]
SiO_x/G/C	Graphite, Pitch	74%	775/653/84/100	524/350	2019	[103]
Si/SiO_x/N−C	Konjac flour	48	1757/1147/65/100	952/100	2019	[104]
SiO_x/C	Sucrose	12	1284/830/65/100	755/300	2019	[69]
SiO_x/ND−C	Citric acid	37	1793/1209/67/100	1182/100	2019	[105]
SiO_x@graphite−Fe	Graphite	—	2331/1139/49/200	757/100	2019	[106]
SiO_x@C	C_2H_4 (CVD)	7	1986/1491/75/1000	1290/500	2019	[107]
SiO_x/C	Hexane	8	1666/1081/65/100	1029/100	2019	[108]
DC−$HSiO_x$	Graphene, phenolic resin	22	1858/1113/60/100	982/200	2019	[70]
SiO_x/graphene	Graphene	—	2091/1326/63/100	1270/120	2019	[109]
rGO@SiO_x@C	rGO, PVP	6	1785/707/40/100	410/200	2020	[110]
N@C/SiO_x	Rice husks	—	2225/1661/72/100	1019/100	2020	[111]
VG@SiO_x/N−C	CH_4 (CVD), graphene	33	1797/1324/74/100	1230/100	2020	[112]
Void@SiO_x@C	Pitch	33	1226/751/61/100	696/500	2020	[99]
SiO_x/C	Bamboo shoot hulls	77	1332/1258/94/200	1289/400	2021	[113]
Si−SiO_x@C	Sugarcane leaves	60	1451/1277/88/200	1562/400	2021	[114]
SiO_x/C	Citric acid	43	1067/684/64/100	721/202	2021	[115]

Note: RF—resorcinol/formaldehyde; MWCNT—multiwall carbon nanotube; PAN—polyacrylonitrile; G—graphite; rGO—reduced graphene oxide; ND—nano-diamond; DC—dual carbon conductive network; VG—vertical graphene; PVP—polyvinylpyrrolidone.

and hexane show a high reversible capacity of 1603 $mAh \cdot g^{-1}$ with a capacity retention of 96.1% at 0.2 $A \cdot g^{-1}$ after 400 cycles [108].

Graphene has a high surface area, superior electronic conductivity, and excellent mechanical flexibility. The incorporation of graphene into SiO_x can increase electronic conductivity, limit the volume change, and improve electrode reaction kinetics and cycling performance. Various SiO_x/graphene composites as anodes for LIBs have been reported. SiO_x/graphene composites with different ratios were prepared from multilayer graphene and SiO_x powders through HEMM [109]. The prepared composite electrode exhibits a reversible capacity of 1326 $mAh \cdot g^{-1}$ with a capacity retention of 95.8% after 120 cycles, which is much higher than that of SiO_x electrodes (capacity retention of 62.6% after 120 cycles). With respect to the SiO_x/graphene composite, the introduction of other carbon components and the design of special structures were also adopted to improve the electrochemical performance of SiO_x anodes. Multicomponent nanosheets rGO-SiO_x@C were prepared (Fig. 5(a)) in a configuration of rGO nanosheets as the substrate, porous SiO_x as the intermediate layer, and nitrogen-doped nanoporous carbon as the shell. The highly porous structure of the composite ensures good cycling stability of the electrode (Fig. 5(a)–(c)) [110]. Similar multicomponent microspheres were prepared by Han *et al*. [112], in which SiOCN microspheres were obtained by pyrolysis of $C_{10}H_{28}N_2OSi_2$, and then graphene (VG) was vertically grown on their surface. The outer porous graphene and inside conductive N-doped carbon enable the multicomponent SiO_x-based microspheres to exhibit an attractive electrochemical performance with a high specific capacity and long-term cyclability (Fig. 5(d)–(f)).

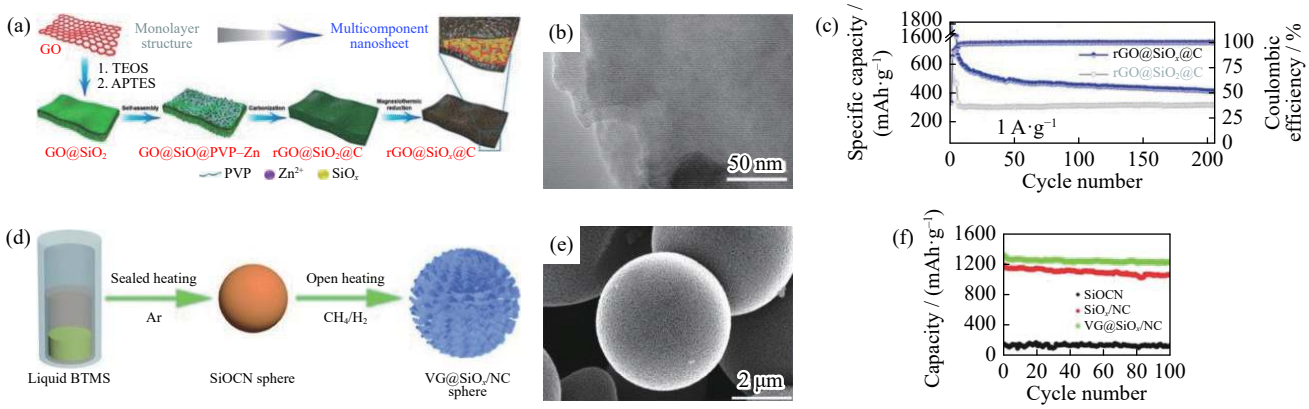

Fig. 5. (a) Schematic of the proposed fabrication route of rGO@SiO_x@C nanosheets; (b) TEM image of rGO@SiO_x@C; (c) CE and cycling stability at a current density of 1 $A \cdot g^{-1}$ of rGO@SiO_2@C and rGO@SiO_x@C; (d) diagram for the synthesis of VG@SiO_x/NC microspheres; (e) SEM image of VG@SiO_x/NC; (f) Comparison of cycling performance of the prepared samples at 0.1 $A \cdot g^{-1}$. (a–c) Reprinted from L.Y. Chen, J. Zheng, S.Y. Lin, S. Khan, J.L. Huang, S.H. Liu, Z.R. Chen, D.C. Wu, and R.W. Fu, Synthesis of SiO_x/C composite nanosheets as high-rate and stable anode materials for lithium-ion batteries, *ACS Appl. Energy Mater*., 3(2020), No. 4, p. 3562. Copyright 2020 American Chemical Society; (d–f) reprinted with permission of Royal Society of Chemistry, from Vertical graphene growth on uniformly dispersed sub-nanoscale SiO_x/N-doped carbon composite microspheres with a 3D conductive network and an ultra-low volume deformation for fast and stable lithium-ion storage, M.S. Han, Y.B. Mu, F. Yuan, J.B. Liang, T. Jiang, X.D. Bai, and J. Yu, 8, Copyright 2020, permission conveyed through Copyright Clearance Center, Inc.

Carbon nanotubes have attracted much attention because of their numerous advantages, including good conductivity, excellent flexibility, high strength, and good stability. Their usage to form composites with SiO_x is expected to strengthen electrical conductivity, homogenize the electrode reaction on the whole electrode surface, enhance the resistance against stress, and therefore improve the cycling performance of the electrode. For example, Guo *et al*. [119] prepared a flexible continuous thin film electrode composed of carbon nanotubes and SiO_x, which show a relatively stable and high specific capacity of ~1240 $mAh \cdot g^{-1}$ after 100 cycles at 100 $mA \cdot g^{-1}$.

5.2.2. SiO_x/metal and SiO_x/metal oxide composites

In addition to combining SiO_x with various carbon materials, compositing SiO_x with metals and metal oxides is another effective way to improve the electrochemical performance of SiO_x electrodes. The metal oxides formed by the reaction of SiO_x and metals can alleviate the large volume changes of SiO_x electrodes during cycling. Moreover, the added metals can enhance the electronic conductivity, which can further improve the charge transfer kinetics of SiO_x anodes.

Wen and other researchers [48,120] prepared a series of nanosized Si-based composites using SiO and metals, such as Li or Ni [121], by using HEMM followed by heat treatment. During milling, nanosized composites consisting of an inactive matrix (Li_2O, Li_4SiO_4, or Ni_2SiO_4) and uniformly distributed active particles (Si or Si–Ni) form (Fig. 6(a)). The inert phases can effectively buffer the volume expansion and enhance the cycling stability of electrodes. The ICE of this type of electrode can be considerably increased at the expense of specific capacity because the oxygen in SiO has been fixed by the addition of metals to form an inactive matrix.

Metals coated on the SiO_x surface can effectively mitigate the pulverization of the electrodes. Apart from enhancing the conductivity, the integrity of the frame structure of the material can be improved with metal nanoparticle coating. This can

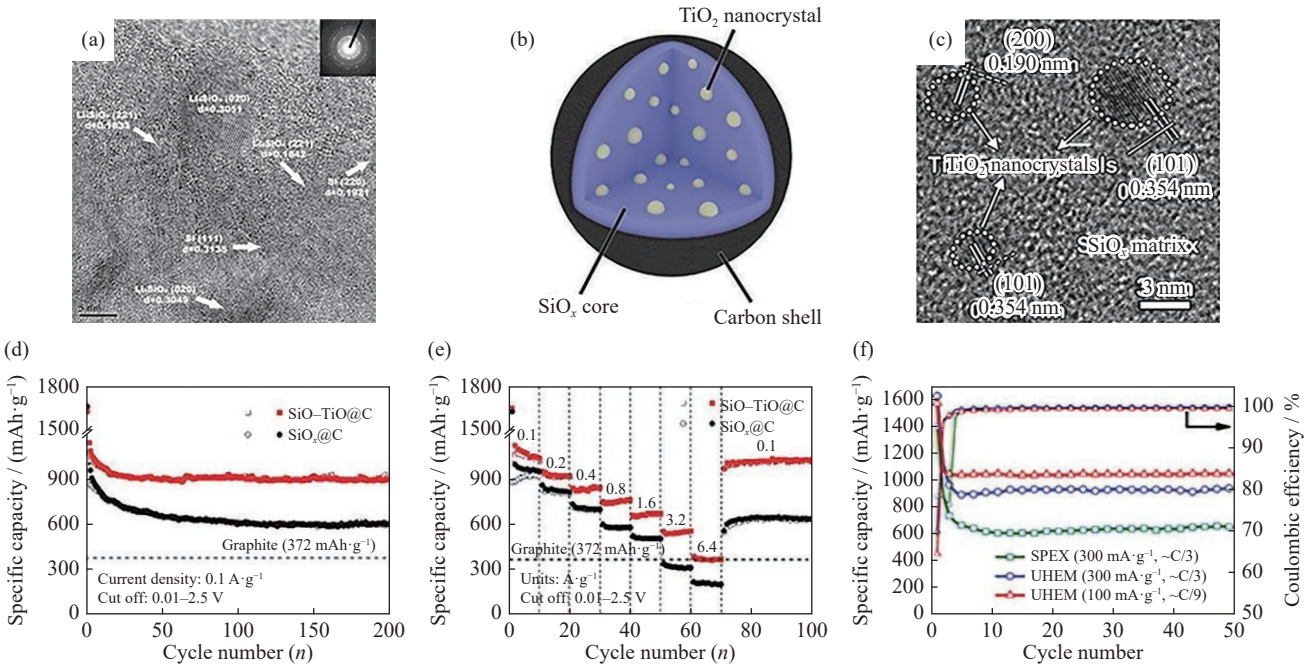

Fig. 6. (a) HRTEM image of the composite powder after milling SiO and lithium metal for 10 h, and the inset of the figure shows clear lattice fringes of Li_4SiO_4; (b) schematic particle structure; (c) HRTEM image; (d) cycle performance; (e) rate performance of SiO_x–TiO_2@C ; (f) cycling performance of cells with UHEM anode (current C/9 and C/3) and SPEX anode (current C/3) at room temperature. (a) Reprinted from *J. Power Sources*, 164, X.L. Yang, Z.Y. Wen, X.X. Xu, B. Lin, and S.H. Huang, Nanosized silicon-based composite derived by in situ mechanochemical reduction for lithium ion batteries, 880-884, Copyright 2007, with permission from Elsevier; (b–e) Z.L. Li, H.L. Zhao, P.P. Lü, Z.J. Zhang, Y. Zhang, Z.H. Du, Y.Q. Teng, L.N. Zhao, and Z.M. Zhu, *Adv. Funct. Mater.*, 28, 1605711 (2018) [73]. Copyright Wiley-VCH Verlag GmbH & Co. KGaA. Reproduced with permission; (f) reprinted from B. Liu, A. Abouimrane, Y. Ren, M. Balasubramanian, D.P. Wang, Z.Z. Fang, and K. Amine, New anode material based on SiO–$Sn_xCo_yC_z$ for lithium batteries, *Chem. Mater.*, 24(2012), No. 24, p. 4653. Copyright 2012 by American Chemical Society.

be attributed to the homogenized electrode reaction on the particle surface enabled by the metal nanoparticles, which ensures a uniform particle volume change and so less structural stress inside the particles. Numerous SiO_x-based composite materials coated with W [122], Cr [123], or Cu [124] have been developed by physical vapor deposition or wet-chemistry methods.

In addition to improving the cycling performance of SiO_x, some additional benefits can be obtained by using metal oxides to form composites. For example, TiO_2 has various merits, including high thermal stability (which helps suppress reactions between SiO_x and the electrolyte), good mechanical properties to endure the volume changes of SiO_x, and low costs. Several SiO_x-based composites have been reported with the addition of TiO_2 [91,125–126]. Li *et al.* [73] designed a watermelon-like structured SiO_x-TiO_2@C nanocomposite by using the sol–gel method (Fig. 6(b)), TiO_2 nanocrystals were evenly embedded inside the SiO_x matrix (Fig. 6(c)). The addition of TiO_2 components effectively improves the electron and lithium-ion conductivity inside SiO_x particles and releases the structural stress occurring in the charge and discharge of SiO_x. The SiO_x–TiO_2@C electrode exhibits stable cycle performance (~910 $mAh·g^{-1}$ after 200 cycles at 0.1 $A·g^{-1}$) and excellent rate performance (Fig. 6(d) and (e)) [73].

Moreover, some other metal oxides, such as Fe_2O_3 [127], ZrO_2 [128], and SnO_2 [129], are employed to improve the cycle performance of SiO_x by increasing the conductivity of the composite and buffering the volume changes during lithiation/delithiation. Liu *et al.* [130] prepared a family of composite anode materials, SiO/$Sn_{30}Co_{30}C_{40}$, consisting of 50wt% SiO and 50wt% $Sn_{30}Co_{30}C_{40}$, by a custom-made ultrahigh-energy ball milling (UHEM) setup. The formed composite materials combine the high capacity of SiO_x and the good cycle performance of $Sn_{30}Co_{30}C_{40}$. Experimental results (Fig. 6(f)) showed that the UHEM SiO/$Sn_{30}Co_{30}C_{40}$ composite electrode delivered reversible capacities of 1040 and 900 $mAh·g^{-1}$ at currents of 100 and 300 $mA·g^{-1}$ after 100 cycles, respectively. Subsequently, Liu *et al.* [131] used a cheaper and environmentally friendly iron instead of expensive and toxic cobalt to prepare SiO/$Sn_xFe_yC_z$ composite anodes through the same method. It was shown that the 50wt% SiO–50wt% $Sn_{30}Fe_{30}C_{40}$ composite electrode delivered reversible capacities of 900 and 700 $mAh·g^{-1}$ at current densities of 300 and 800 $mA·g^{-1}$, respectively. Table 2 summarizes the representative electrochemical performance of SiO_x/metal and SiO_x/metal oxide composite anodes.

5.3. Electrolyte additives for stabilization of SEI film on SiO_x electrodes

The discussed above serious problem related to the instability of SEI formed on SiO_x materials can be addressed by proper usage of the liquid electrolyte additives. In fact, the degradation of a battery involves the active material and the

Table 2. Electrochemical performance of SiO_x/metal and SiO_x/metal oxide composite electrodes

Anode material	Initial discharge capacity ($mAh \cdot g^{-1}$)/ Charge capacity ($mAh \cdot g^{-1}$)/Coulombic efficiency (%)/ Current density	Stable capacity ($mAh \cdot g^{-1}$)/ Number of cycles	Year	Ref.
SiO/Li	951/770/81/0.1 $mA \cdot cm^{-2}$	762/50	2007	[132]
SiO/SnO/Li	1338/901/67/0.1 $mA \cdot cm^{-2}$	574/200	2009	[90]
$SiO/Sn_{30}Co_{30}C_{40}$	1030/1480/70%/300 $mA \cdot g^{-1}$	900/300	2012	[130]
$SiO/Sn_{30}Fe_{30}C_{40}$	1343/900/67/300 $mA \cdot g^{-1}$	900/50	2013	[131]
SiO/Fe_2O_3	2773/1893/68/160 $mA \cdot g^{-1}$	1335/50	2013	[127]
$C/Cr/SiO_x$	780/591/76%/0.5 C	490/50	2014	[123]
SiO/W/graphite	964/566/59/0.5 C	358/100	2015	[122]
$SiO/ZrO_2/C$	1737/1157/67/80 $mA \cdot g^{-1}$	721/100	2016	[128]
SiO/Cu/graphite	1177/2473/48/50 $mA \cdot g^{-1}$	836/100	2017	[124]
SiO/TiO_2	1070/137/78/100 $mA \cdot g^{-1}$	730/100	2019	[125]
$SiO_x/SnO_2/C$	2186/1158/53/100 $mA \cdot g^{-1}$	1127/100	2020	[129]

electrolyte. Regarding typically used liquid electrolytes, Lin *et al*. [133] found that $LiPF_6$ salt can be hydrolyzed even in the presence of a small number of water molecules, which generates harmful HF [Eqs. (1)–(3)] [133–134]:

$$LiPF_6 \rightarrow LiF + PF_5 \quad (1)$$

$$PF_5 + H_2O \rightarrow POF_3 + 2HF \quad (2)$$

$$POF_3 + H_2O \rightarrow HPO_2F_2 + HF \quad (3)$$

The strong tendency of Si to form Si–F bonds promotes the reaction between SiO and HF, which produces more H_2O and thus causes further hydrolysis of $LiPF_6$ [134]. This process can destroy the carbon layer on the surface of SiO and prevents the formation of the stable SEI film, which ultimately leads to the ongoing destruction of the electrode.

Electrolyte additives are the most simple, economical, effective, and feasible way to help construct a stable SEI film on anode materials, preventing the continuous decomposition of the electrolyte [135]. Mitigating the damage of HF on SiO_x anodes is also crucial for the cycling performance of SiO_x-based electrodes.

Vinylene carbonate (VC) and fluoroethylene carbonate (FEC) are the most widely used additives in SiO_x-based LIBs [27,136–138]. VC was first reported as the additive for Si-based LIBs by Chen *et al*. [139] in 2006. Such addition facilitates the formation of a uniform, smooth, and flexible SEI film with polycarbonate as the main component to withstand the volume changes of SiO_x [134]. FEC can also form a stable SEI film on the surface of Si, which prevents the penetration of the electrolyte breaking the –Si–Si– network bonds [140] and restricts the decomposition of the electrolyte, the oxidation of Si [141], and even the diffusion of HF to some extent [142]. The main components in the SEI film formed by FEC are LiF and polyene compounds. LiF nanocrystals not only have well Li^+ conductivity but also can enhance Li^+ conductivity by the creation of interface defects between LiF and the organic matrix in the SEI film, which improves the rate performance of SiO_x electrodes [134,141]. However, VC and FEC have their own limitations. The VC additive usually causes a dense SEI film, which blocks the migration of Li^+ and so limits the power density of the battery. The film formed by FEC is less flexible and cannot fit well with the volume changes of SiO_x, thus reducing the cycle life [134]. Our group employed $LiNO_3$ and VC as synergistic additives for electrodes and electrolytes, respectively, to improve the electrode/electrolyte interface properties. The reduction products of Li_3N and LiN_xO_y from $LiNO_3$ and polycarbonate from VC endow the SEI film with high ionic conductivity and enhanced elasticity, which enable a fast and uniform electrode reaction. The synergistic effect of $LiNO_3$ and VC enables the bare SiO electrode to deliver a high reversible capacity of 1062.3 $mAh \cdot g^{-1}$ and an excellent cycling performance with 94.5% capacity retention and 99.80% coulombic efficiency for 160 cycles [143].

Many functional electrolyte or electrode additives have been developed to promote the formation of stable and firm SEI film. For example, LiF was introduced into the electrode to compensate for the Li^+ consumption during SEI film formation [116]. 4,5-Difluoro-1,3-dioxolan-2-one shows strong electronegativity because of the two fluorine elements and thus can be easily reduced to form a solid SEI film on the electrode surface, thus improving the cycling performance of SiO_x electrodes [144]. LiBOB can decompose to form a more resistive SEI film, which can control the alloying depth of SiO and prevent the formation of crystalline $Li_{15}Si_4$ phase, thus improving the cycling performance of SiO electrodes [145]. Moreover, LiTFSI/Py13-TFSI can passivate the SiO_x electrode surface to form a stable, dense, and flat SEI film composed of pyrrolidinium, TFSI ions, and their decomposition products, effectively improving the cycling life of SiO_x-based anodes [146].

5.4. Methods for overcoming the low ICE of SiO_x-based anodes

In the initial lithiation of SiO_x, the ICE of the SiO_x anode can be much lower than that of pure Si or graphite because of the formation of the SEI and irreversible phases, such as Li_2O, Li_4SiO_4, and other lithium silicates. A large part of Li ions from the electrolyte and cathode is immobilized in the first lithiation, decreasing the availability of lithium and significantly restricting the practical applications of SiO_x. Many

effective methods have been proposed to mitigate this fundamental problem. At present, the two most important strategies are prelithiation and prereduction.

5.4.1. Prelithiation methods

Prelithiation is a viable method to offset the irreversible Li consumption during cycling by introducing extra Li into electrodes in advance. The effective approaches reported include direct contact with metal lithium, chemical and electrochemical prelithiation, and cathode-side prelithiation.

(I) Direct addition of metal lithium powders.

Direct addition of metal lithium powders into the SiO_x electrode is commonly adopted for Si-based anodes to compensate for the large irreversible lithium consumption. The direct contact of metal lithium with active SiO_x particles makes SiO_x partially prelithiated, which allows the generation of irreversible products before the lithium comes from the cathode during the initial charge. This phenomenon avoids the irreversible consumption of cathode lithium. Stable lithium metal powder (SLMP) is an efficient prelithiation agent composed of lithium carbonate and lithium metal powder [48]. Li metal particles are uniformly coated by lithium carbonate, which forms a protective layer to handle the material in dry air safely. As such, pressure must be applied to break the lithium carbonate layer in the prelithiation procedure to activate the lithium metal powder. The complete process of the SLMP route is shown in Fig. 7(a) [147]. In 2005, Jarvis *et al*. [148] first reported the application of SLMP in the graphite anode for LIBs. By introducing 1.93wt% SLMP, the ICE of the graphite anode could increase from 77.9% to 95.4%, demonstrating the high effectiveness of this approach. Subsequently, SLMP prelithiation was applied to several LIB anodes, including Si [149] and SiO_x [150–151]. With 15wt% SLMP added, the ICE of a micro-sized SiO-based anode was improved from 68.1% to 98.5% [150].

Due to the high specific capacity of metallic lithium (3860 $mAh \cdot g^{-1}$), only a small amount of SLMP is sufficient to realize the prelithiation of SiO_x electrodes. Furthermore, SLMP has important advantages related to the facile and controllable prelithiation route. However, the high cost, environmental pollution, and potential safety problems limit its wide application.

(II) Chemical prelithiation.

As early as 2005, Tabuchi *et al*. [152] developed a Li-doped SiO active material (Li_xSiO) with the reduced irreversible capacity by a process involving the dissolution of naphthalene and metallic Li into butyl methyl ether solvent to form a Li-organic complex solution and then immersing the SiO electrodes in the abovementioned solution. It is a facile method to compensate for the irreversible lithium-ion loss that the anode materials react with reductive prelithiation reagents directly. The degree of prelithiation can be tuned by the immersion time. The process of chemical prelithiation is shown schematically in Fig. 7(b) [153].

In recent years, many prelithiation reagents have been exploited to improve the ICE of negative electrodes [152–154], and considerable progress has been made. Yan *et al*. [155] reported an effective strategy to achieve the uniform pre-lithiation of SiO_x/C microparticles by mixing with a lithium-biphenyl complex solution so that the ICE of half-cell was as high as 90%. However, such reagents usually show high reactivity in ambient air, which is challenging for practical applications.

(III) Electrochemical prelithiation.

The electrochemical approach is a relatively simple method to achieve the prelithiation of SiO_x electrodes. It can be divided into direct and indirect contact prelithiation routes [156–159].

When the lithium foil is in direct contact with SiO_x electrodes with also a presence of the electrolyte, electrons transfer from Li metal to SiO_x, with concurrent insertion of Li^+, because of the potential difference between the lithium foil and SiO_x electrode, achieving the required prelithiation [156–157]. The method is simple and operable, but the prelithiation depth and uniformity are not satisfactory. In 2019, Meng *et al*. [158] optimized the prelithiation of the direct contact of the anode and Li foil, proposing to add a resistance buffer layer (RBL) between the Li foil and SiO_x electrode to achieve uniform prelithiation. The rate and depth of lithiation can be adjusted by controlling the resistance of RBL and the time of the process. When assembled in a full cell with NCM622 cathode, the ICE of the prelithiated NCM622-SiO_x full cell can increase from 68.9% to 87.3% with respect to the one without prelithiation.

As for the indirect contact prelithiation, a temporary battery must be constructed using SiO_x and Li metal as the positive and negative electrodes, respectively. The SiO_x electrode is discharged with a specific current to achieve the insertion of Li^+ [159]. The degree of prelithiation can be controlled by circuit parameters, such as voltage and current density. However, constructing a temporary battery is time-consuming and brings additional costs, which is unrealistic for commercial applications. To overcome this issue, Kim *et al*. [159] proposed a modified electrochemical prelithiation where pressure on a temporary constructed cell was applied, and a roll-to-roll manufacturing line was employed, as shown in Fig. 7(c). The degree of prelithiation can be accurately tuned by controlling short circuit time and monitoring voltage. When the resistance reached 100 Ω and the short circuit time was 30 min, the carbon-coated SiO_x (denoted as c-SiO_x) electrode showed an optimized ICE of 94.9%. When assembled with NCA cathode, the energy density of the prelithiated c-SiO_x/NCA full cell was 155% higher than that of the pristine c-SiO_x/NCA battery.

(IV) Cathode-side prelithiation.

The ICE of SiO_x can be improved by introducing Li-containing cathode additives. As shown in Fig. 7(d) [160], the introduction of such additives can effectively compensate for the irreversible capacity loss of SiO_x and reduce the Li^+ loss of the cathode. Cathode additives, such as Li_6CoO_4 [160], Li_3N [161], and Li_2O_2 [162], could supply extra lithium to compensate for the irreversible capacity loss of the anode. Noh and Cho [160] assembled a $LiCoO_2$/SiO_x full cell with 15wt% Li_6CoO_4 added to the $LiCoO_2$ cathode, which exhib-

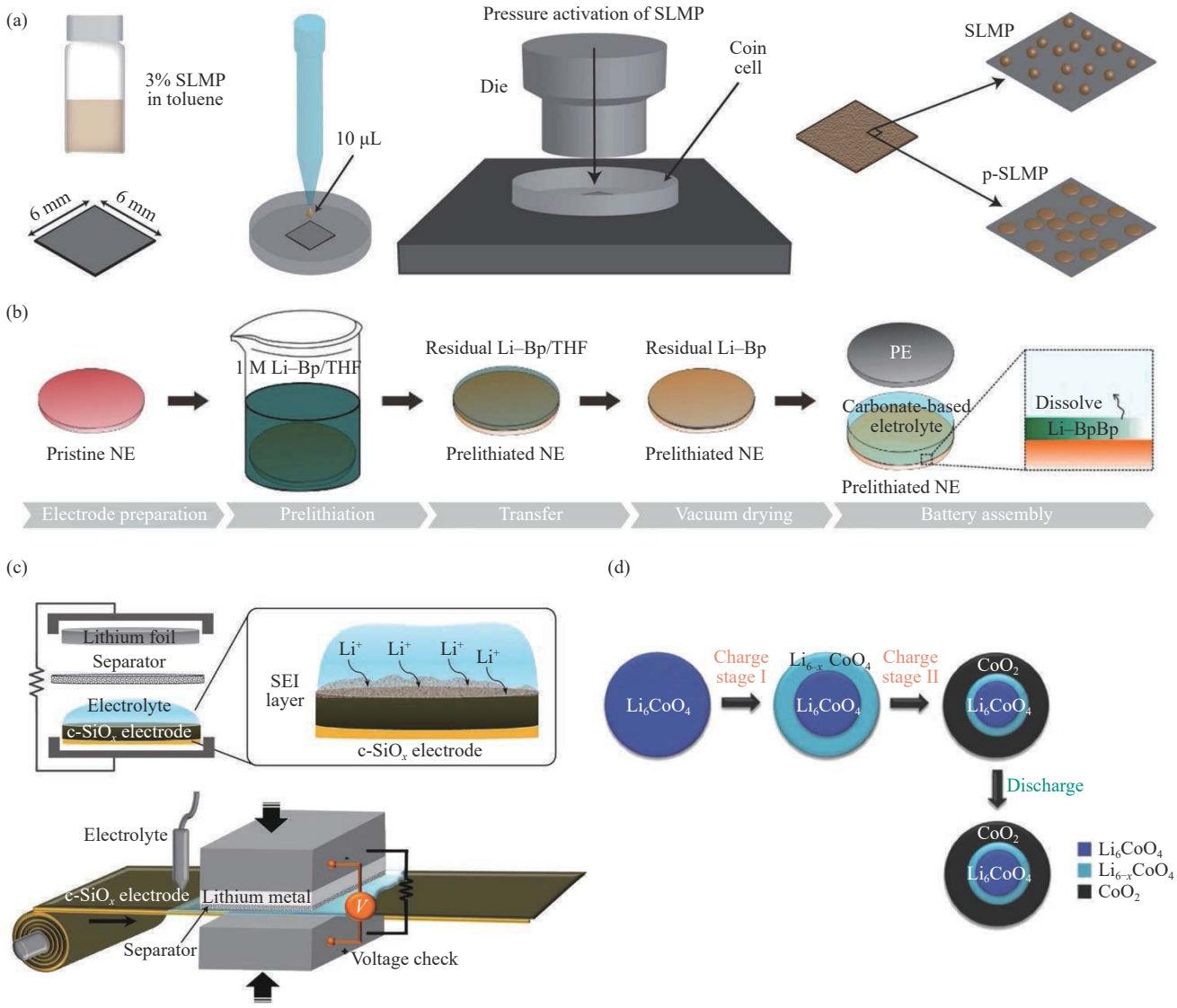

Fig. 7. Schematic of different prelithiation procedures: (a) SLMP; (b) chemical one; (c) electrochemical prelithiation and its scaled-up roll-to-roll process scheme; (d) schematic for the electrochemical reaction of prelithiation reagent Li_6CoO_4. (a) Reprinted from M.W. Forney, M.J. Ganter, J.W. Staub, R.D. Ridgley, and B.J. Landi, Prelithiation of silicon-carbon nanotube anodes for lithium ion batteries by stabilized lithium metal powder (SLMP), *Nano Lett.*, 13(2013), No. 9, p. 4158. Copyright 2013 by American Chemical Society; (b) reprinted from G.W. Wang, F.F. Li, D. Liu, D. Zheng, Y. Luo, D.Y. Qu, T.Y. Ding, and D.Y. Qu, Chemical prelithiation of negative electrodes in ambient air for advanced lithium-ion batteries, *ACS Appl. Mater. Interfaces*, 11(2019), No. 9, p. 8699. Copyright 2019 by American Chemical Society; (c) reprinted from H.J. Kim, S. Choi, S.J. Lee, M.W. Seo, J.G. Lee, E. Deniz, Y.J. Lee, E.K. Kim, and J.W. Choi, Controlled prelithiation of silicon monoxide for high performance lithium-ion rechargeable full cells, *Nano Lett.*, 16(2016), No. 1, p. 282. Copyright 2016 by American Chemical Society; (d) reprinted from M. Noh and J. Cho, *J. Electrochem. Soc.*, 159(2012) [160]. ©IOP Publishing. Reproduced with permission. All rights reserved.

its a reversible capacity ratio from 43% to 66%.

In general, cathode-side prelithiation provides more options for improving the ICE of SiO_x. Different additives should be matched with the potential of the cathodes so that the extra-lithium can be released in the charge window. Moreover, the additive amount should be well-controlled.

5.4.2. Prereduction method

As discussed above, in the initial lithiation process, the irreversible capacity loss of SiO_x mainly comes from the side reactions between Li and SiO_x and the formation of SEI. The former contributes a large part of irreversible capacity because of the formation of various electrochemically inactive lithium silicates and lithium oxide. As such, the initial oxygen amount x in the material strongly influences such capacity loss [120]. Therefore, SiO_x reduction by reacting with reductive metals, such as Al [163], Li [48,120], and Ni [121], has been proposed to form metal oxides and silicates. Apart from decreasing the x value of SiO_x and avoiding the lithium consumption from oxygen, the formed metal oxides and silicates can buffer the volume changes of SiO_x to improve its cycle performance.

Jeong *et al.* [163] prepared a nanostructured composite material with chemical composition $SiAl_{0.2}O$ through HEMM using SiO powder and Al metal powder as the raw materials. The SiO_2 in the disproportionated SiO can be reduced to Si, and the electrochemically inactive Al_2O_3 is gen-

erated in HEMM, which can mitigate the cracking and fracture of the active material in the cycling process. It was shown that such formed $SiAl_{0.2}O$ composite was composed of silicon nanocrystallites and an amorphous matrix consisting of SiO_2 and Al_2O_3. The ICE was increased by 10% when compared with unmodified SiO, and the $SiAl_{0.2}O$ material exhibited a stable cycling performance with a reversible capacity of 800 $mAh \cdot g^{-1}$ over 100 cycles at 120 $mA \cdot g^{-1}$.

5.5. Alleviation of the macro-cracking effect of SiO_x electrodes

It is of great importance to ensure tight bonding of SiO_x particles and the conductive agent between each other, and with the current collector, to prevent loss of electrical contact. However, providing sufficient adhesion to maintain electrode integrity under large volume changes upon cycling is difficult because of the weak Van der Waals forces between SiO_x and typically used polyvinylidene fluoride (PVDF) binders. In addition, the usage of PVDF results in strong swelling and the toxicity of concomitant solvent N-methyl-2-pyrrolidone. Various binders have been employed in SiO_x-based electrodes and can be classified into two categories based on their functions: (1) improvement of adhesion through hydrogen bonding between the binder and SiO_x and (2) formation of a 3D cross-linked network to improve the mechanical properties of the electrode.

5.5.1. Hydrogen bonding for improving adhesion

The Van der Waals force between the binder and the SiO_x particle is a weak intermolecular force. Thus, it can be easily destroyed by large volume changes. By contrast, the hydrogen bond is relatively strong and shows some self-healing function in volume change environments [164–165]. Therefore, the design of binders with functional groups that can form hydrogen bonds with SiO_x particles has become an important aspect for the deployment of SiO_x in LIBs.

Sodium carboxymethyl cellulose (CMC) and sodium alginate (Alg) have been adopted as binders in SiO_x electrodes; these binders, which benefit from the presence of polar groups on their molecular chains, can provide stronger adhesion than PVDF by forming abundant hydrogen bonds [156,166–167]. This phenomenon is also widely observed in other biomass-originating binders, such as xanthan gum [168], guar gum [169], chitosan [170], β-cyclodextrin [171], and konjac glucomannan (KGM) [26]. For example, compared with Alg, KGM can form more hydrogen bonds with Si–OH on the surface of $Si@SiO_2$. Molecular mechanics simulation revealed that the interfacial adhesion energy between KGM and $Si@SiO_2$ is 0.205 $J \cdot m^{-2}$, which is 0.018 $J \cdot m^{-2}$ higher than that of Alg (Fig. 8(a) and (b)). The strong adhesion of binder with SiO_x active particle and the self-healing ability of hydrogen bond make the electrode tolerant to the mechanical stress caused by the large volume change in SiO_x upon lithiation/delithiation. Some other non-biomass adhesives, including poly(acrylic acid) (PAA) [172–173], polyvinyl alcohol (PVA) [174–175], and polyacrylamide [176], exhibit similar functions and can be used to improve electrode integrity.

5.5.2. Formation of 3D cross-linked network

Morphological analysis suggests that the contact between binders and active materials has three main types: point–

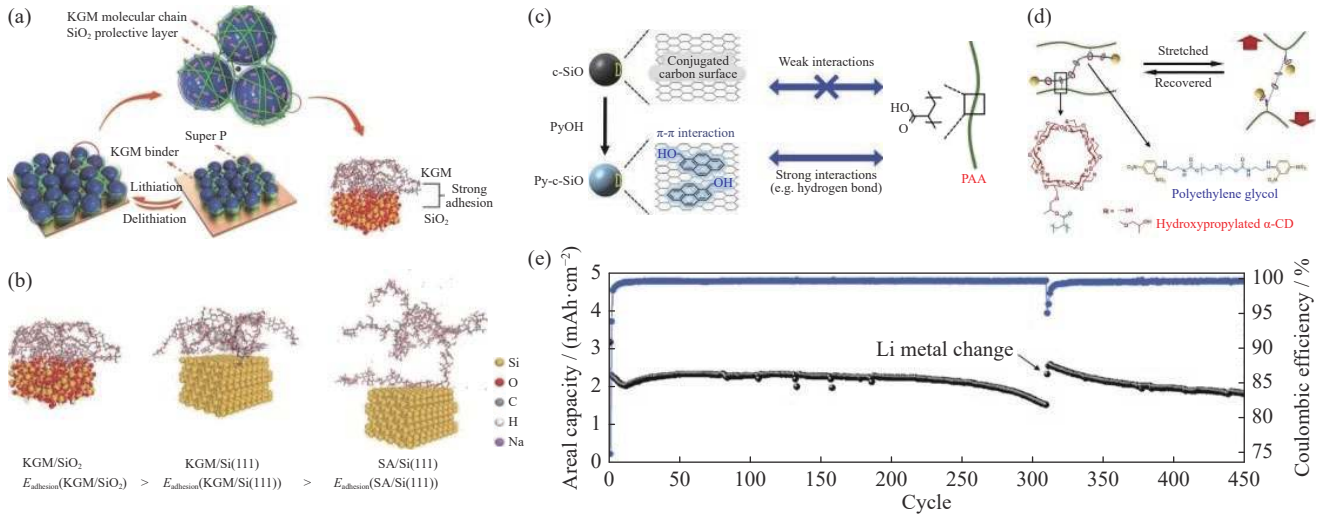

Fig. 8. (a) Schematic of lithiation and delithiation for KGM/$Si@SiO_2$: the surface oxide layer of SiO_2 on Si nanoparticles enhances the interfacial adhesion with the KGM binder, and it protects the Si cores; (b) structures of KGM/SiO_2, KGM/Si(111), and SA/Si(111) model systems from molecular mechanics simulation; (c) schematic of surface modification of c-SiO using PyOH and its interaction with PAA; (d) Ring-sliding motion in PRPAA and its chemical structure; (e) cycling performance of Py-c-SiO-PRPAA electrode at 1.78 $mA \cdot cm^{-2}$. (a, b) S.T. Guo, H. Li, Y.Q. Li, Y. Han, K.B. Chen, G.Z. Xu, Y.J. Zhu, and X.L. Hu, SiO_2-enhanced structural stability and strong adhesion with a new binder of konjac glucomannan enables stable cycling of silicon anodes for lithium-ion batteries, *Adv. Energy Mater.*, 8, 1800434 (2018) [26]. Copyright Wiley-VCH Verlag GmbH & Co. KGaA. Reproduced with permission; (c, d) Y. Cho, J. Kim, A. Elabd, S. Choi, K. Park, T.W. Kwon, J. Lee, K. Char, A. Coskun, and J.W. Choi, A pyrene–poly(acrylic acid)–polyrotaxane supramolecular binder network for high-performance silicon negative electrodes, *Adv. Mater.*, 31, 1905048 (2019) [178]. Copyright Wiley-VCH Verlag GmbH & Co. KGaA. Reproduced with permission.

point, point-line, and point–net. The point–point shows the smallest contact area and the weakest adhesion. This contact type mainly involves styrene-butadiene rubber and poly(tetrafluoroethylene) binders. Most of the single-polymer adhesives form the point-line contact, which provides a large combination area and considerable adhesion strength. Among them, PVDF, CMC, Alg, PAA, and PVA are typical examples. Although the adhesion area of the point-net contact type is not much larger than that of the point-line contact type, it can effectively accommodate the volume changes in SiO_x through the deformation between the branches to form a 3D bonding network, showing the best adhesion performance [177]. Therefore, forming a cross-linked 3D adhesive network is another important area regarding the development of high-performance binders.

PAA is a widely used material for 3D cross-linked network construction. It can not only form hydrogen bonds with SiO_x particles but also partly bridge and cross-link itself by carboxylic groups in PAA molecules, forming a 3D network that could accommodate the large volume changes of SiO_x [172]. However, PAA is apt to self-polymerize to form stiff bundles through carboxyl groups, which would reduce the contact sites of the binder with active SiO_x particles. He *et al*. [99] in situ cross-linked polyacrylic acid and d-sorbitol binder to form a 3D network structure, which enables the SiO electrode to have improved cycling stability than that with PAA by providing more contact sites for active particles. In another research, Cho *et al*. [178] prepared polyrotaxane cross-linked PAA (PRPAA) as a binder. PRPAA is composed of cyclodextrin rings and poly(ethylene glycol) chains. Cyclodextrin rings covalently cross-link to PAA through the ester linkage and thread along the poly(ethylene glycol) chain, providing a sliding motion effect (Fig. 8(c) and (d)), which ensures a good elasticity of this binder. Based on this design, 1-pyrenemethanol (PyOH)-modified carbon-coated SiO (c-SiO) electrode with mass loading between 2.3 and 2.5 mg preserves a capacity of approximately 2.54 $mAh \cdot cm^{-2}$ with 97.6% capacity retention after 100 cycles at 1.78 $mA \cdot cm^{-2}$. In addition, 92.6% capacity retention was achieved after 250 cycles (Fig. 8(e))

6. Conclusions and outlook

Without a doubt, SiO_x is the most potential anode material for high-energy-density LIBs, owing to the high specific capacity and manageable volume changes in lithiation/delithiation processes. However, several challenges remain toward the practical deployment of SiO_x in LIBs, including low ICE and poor cycling performance. The latter is associated with particle pulverization, unstable SEI film, and electrode cracking failure. To overcome these issues, great efforts have been exerted in recent years, which resulted in significant advancements in the electrochemical performance of SiO_x-based anodes.

A series of novel structures and composites was designed to overcome the material pulverization caused by volume changes. Introducing free space and combining SiO_x with the conducting phase (different forms of carbon, metallic elements, MO_x, and so on) are effective ways to improve electrochemical performance. The synthetic technical routes and specific processing parameters have a strong influence on particle morphology, microstructure, and chemical compositions (x value), which decisively affect the electrochemical performance demonstration of SiO_x-based electrodes.

The development of additives and novel binders is an important direction to improve the performance of SiO_x-based anodes. Additives for electrolytes or electrodes can enhance the stability of the SEI film on SiO_x and reduce the continuous consumption of the electrolyte. Meanwhile, the undesirable thickening of the SEI film and the increase in the internal resistance of the battery can be avoided. Apart from exploring novel additives, a combination of different electrolyte additives could be effective and useful. Binders maintain electrode integrity and relieve the performance degradation due to loss of the electrical contact between the active material and the conductive agent or the current collector. Future works could focus on the exploration of new binders with specific groups that have high adhesion energy with SiO_x/Si, self-healing function, and/or the ability to form a 3D cross-linked network. Functional conductive binders are also meaningful.

Prelithiation and prereduction are efficient ways to overcome the low ICE of SiO_x electrodes. Prelithiation technologies include the direct addition of metal lithium powders or prelithiation agents, chemical reaction, electrochemical prelithiation, and cathode-side prelithiation. Prereduction of SiO_x with metal is another route to increase the ICE and improve the cycle performance of SiO_x electrodes. In this regard, the cost, safety, and scalability are crucial factors affecting the practical application of these techniques in SiO_x-involved batteries.

Although SiO_x anodes are still facing critical challenges in route to commercialization, significant progress has been achieved in electrochemical performance in recent years. Future breakthroughs most likely related to the development of simple and low-cost synthesis routes and the overall improvement of the performance of SiO_x anodes shall ensure their wide usage in next-generation high-energy-density LIBs.

Acknowledgements

This work was financially supported by the National Natural Science Foundation of China (Nos. U1637202 and 52074023), the National Key R&D Program of China (No. 2018YFB0905600), and the Beijing Municipal Education Commission-Natural Science Foundation Joint Key Project (No. KZ201910005003).

Conflict of Interest

The authors declared that they have no conflicts of interest.

References

[1] T.H. Kim, J.S. Park, S.K. Chang, S. Choi, J.H. Ryu, and H.K. Song, The current move of lithium ion batteries towards the next phase, *Adv. Energy Mater.*, 2(2012), No. 7, p. 860.

[2] G.E. Blomgren, The development and future of lithium ion batteries, *J. Electrochem. Soc.*, 164(2016), No. 1, p. A5019.

[3] Y. Yamada, K. Usui, C.H. Chiang, K. Kikuchi, K. Furukawa, and A. Yamada, General observation of lithium intercalation into graphite in ethylene-carbonate-free superconcentrated electrolytes, *ACS Appl. Mater. Interfaces*, 6(2014), No. 14, p. 10892.

[4] W.H. Li, X.L. Sun, and Y. Yu, Si-, Ge-, Sn-based anode materials for lithium-ion batteries: From structure design to electrochemical performance, *Small Methods*, 1(2017), No. 3, art. No. 1600037.

[5] D.Q. Liu, Z.J. Liu, X.W. Li, W.H. Xie, Q. Wang, Q.M. Liu, Y.J. Fu, and D.Y. He, Group IVA element (Si, Ge, Sn)-based alloying/dealloying anodes as negative electrodes for full-cell lithium-ion batteries, *Small*, 13(2017), No. 45, art. No. 1702000.

[6] E. Radvanyi, W. Porcher, E.D. Vito, A. Montani, S. Franger, and S. Jouanneau Si Larbi, Failure mechanisms of nano-silicon anodes upon cycling: An electrode porosity evolution model, *Phys. Chem. Chem. Phys.*, 16(2014), No. 32, p. 17142.

[7] M.T. McDowell, S.W. Lee, W.D. Nix, and Y. Cui, 25th anniversary article: Understanding the lithiation of silicon and other alloying anodes for lithium-ion batteries, *Adv. Mater.*, 25(2013), No. 36, p. 4966.

[8] Z.Y. Feng, W.J. Peng, Z.X. Wang, H.J. Guo, X.H. Li, G.C. Yan, and J.X. Wang, Review of silicon-based alloys for lithium-ion battery anodes, *Int. J. Miner. Metall. Mater.*, 28(2021), No. 10, p. 1549.

[9] D.A. Agyeman, K. Song, G.H. Lee, M. Park, and Y.M. Kang, Carbon-coated Si nanoparticles anchored between reduced graphene oxides as an extremely reversible anode material for high energy-density Li-ion battery, *Adv. Energy Mater.*, 6(2016), No. 20, art. No. 1600904.

[10] U. Kasavajjula, C.S. Wang, and A.J. Appleby, Nano- and bulk-silicon-based insertion anodes for lithium-ion secondary cells, *J. Power Sources*, 163(2007), No. 2, p. 1003.

[11] Q. Liu, Z. Cui, R.J. Zou, J.H. Zhang, K.B. Xu, and J.Q. Hu, Surface coating constraint induced anisotropic swelling of silicon in Si–void@SiO_x nanowire anode for lithium-ion batteries, *Small*, 13(2017), No. 13, art. No. 1603754.

[12] W.F. Ren, Y.H. Wang, Q.Q. Tan, J. Yu, U.J. Etim, Z.Y. Zhong, and F.B. Su, Nanosized Si particles with rich surface organic functional groups as high-performance Li-battery anodes, *Electrochim. Acta*, 320(2019), art. No. 134625.

[13] M.X. Chen, W.Y. Cao, L.C. Wang, X. Ma, and K. Han, Chessboard-like silicon/graphite anodes with high cycling stability toward practical lithium-ion batteries, *ACS Appl. Energy Mater.*, 4(2021), No. 1, p. 775.

[14] H.P. Jia, C. Stock, R. Kloepsch, X. He, J.P. Badillo, O. Fromm, B. Vortmann, M. Winter, and T. Placke, Facile synthesis and lithium storage properties of a porous $NiSi_2$/Si/carbon composite anode material for lithium-ion batteries, *ACS Appl. Mater. Interfaces*, 7(2015), No. 3, p. 1508.

[15] Q.K. Du, Q.X. Wu, H.X. Wang, X.J. Meng, Z.K. Ji, S. Zhao, W.W. Zhu, C. Liu, M. Ling, and C.D. Liang, Carbon dot-modified silicon nanoparticles for lithium-ion batteries, *Int. J. Miner. Metall. Mater.*, 28(2021), No. 10, p. 1603.

[16] S. Kim, Y.K. Jeong, Y. Wang, H. Lee, and J.W. Choi, A "sticky" mucin-inspired DNA-polysaccharide binder for silicon and silicon-graphite blended anodes in lithium-ion batteries, *Adv. Mater.*, 30(2018), No. 26, art. No. 1707594.

[17] J.H. Xiong, N. Dupré, D. Mazouzi, D. Guyomard, L. Roué, and B. Lestriez, Influence of the polyacrylic acid binder neutralization degree on the initial electrochemical behavior of a silicon/graphite electrode, *ACS Appl. Mater. Interfaces*, 13(2021), No. 24, p. 28304.

[18] M. Miyachi, H. Yamamoto, and H. Kawai, Electrochemical properties and chemical structures of metal-doped SiO anodes for Li-ion rechargeable batteries, *J. Electrochem. Soc.*, 154(2007), No. 4, art. No. A376.

[19] H. Takezawa, K. Iwamoto, S. Ito, and H. Yoshizawa, Electrochemical behaviors of nonstoichiometric silicon suboxides (SiO_x) film prepared by reactive evaporation for lithium rechargeable batteries, *J. Power Sources*, 244(2013), p. 149.

[20] S.C. Jung, H.J. Kim, J.H. Kim, and Y.K. Han, Atomic-level understanding toward a high-capacity and high-power silicon oxide (SiO) material, *J. Phys. Chem. C*, 120(2016), No. 2, p. 886.

[21] P.P. Lü, H.L. Zhao, Z.L. Li, C.H. Gao, and Y. Zhang, Citrate-nitrate gel combustion synthesis of micro/nanostructured SiO_x/C composite as high-performance lithium-ion battery anode, *Solid State Ionics*, 340(2019), art. No. 115024.

[22] H. Guo, R. Mao, X.J. Yang, and J. Chen, Hollow nanotubular SiO_x templated by cellulose fibers for lithium ion batteries, *Electrochim. Acta*, 74(2012), p. 271.

[23] H.Q. Wang, X.Q. Que, Y.N. Liu, X.X. Wu, Q.H. Yuan, J.Y. Lu, and W. Gan, Facile synthesis of yolk-shell structured Si_xO_x/C@void@C nanospheres as anode for lithium-ion batteries, *J. Alloys Compd.*, 874(2021), art. No. 159913.

[24] W.J. Zhang, Y.Q. Weng, W.C. Shen, R.T. Lü, F.Y. Kang, and Z.H. Huang, Scalable synthesis of lotus-seed-pod-like Si/SiOx@CNF: Applications in freestanding electrode and flexible full lithium-ion batteries, *Carbon*, 158(2020), p. 163.

[25] Y.J. Cai, Y.Y. Li, B.Y. Jin, A. Ali, M. Ling, D.G. Cheng, J.G. Lu, Y. Hou, Q.G. He, X.L. Zhan, F.Q. Chen, and Q.H. Zhang, Dual cross-linked fluorinated binder network for high-performance silicon and silicon oxide based anodes in lithium-ion batteries, *ACS Appl. Mater. Interfaces*, 11(2019), No. 50, p. 46800.

[26] S.T. Guo, H. Li, Y.Q. Li, Y. Han, K.B. Chen, G.Z. Xu, Y.J. Zhu, and X.L. Hu, SiO_2-enhanced structural stability and strong adhesion with a new binder of konjac glucomannan enables stable cycling of silicon anodes for lithium-ion batteries, *Adv. Energy Mater.*, 8(2018), No. 24, art. No. 1800434.

[27] J. Kirner, Y. Qin, L.H. Zhang, A. Jansen, and W.Q. Lu, Optimization of Graphite-SiO blend electrodes for lithium-ion batteries: Stable cycling enabled by single-walled carbon nanotube conductive additive, *J. Power Sources*, 450(2020), art. No. 227711.

[28] H.R. Philipp, Optical properties of non-crystalline Si, SiO, SiO_x and SiO_2, *J. Phys. Chem. Solids*, 32(1971), No. 8, p. 1935.

[29] H.R. Philipp, Optical and bonding model for non-crystalline SiO_x and SiO_xN_y materials, *J. Non Cryst. Solids*, 8-10(1972), p. 627.

[30] R.J. Temkin, An analysis of the radial distribution function of SiO_x, *J. Non Cryst. Solids*, 17(1975), No. 2, p. 215.

[31] M. Nakamura, Y. Mochizuki, K. Usami, Y. Itoh, and T. Nozaki, Infrared absorption spectra and compositions of evaporated silicon oxides (SiO_x), *Solid State Commun.*, 50(1984), No. 12, p. 1079.

[32] K. Schulmeister and W. Mader, TEM investigation on the structure of amorphous silicon monoxide, *J. Non-Cryst. Solids*, 320(2003), No. 1-3, p. 143.

[33] A. Hohl, T. Wieder, P.A. van Aken, T.E. Weirich, G. Denninger, M. Vidal, S. Oswald, C. Deneke, J. Mayer, and H. Fuess, An interface clusters mixture model for the structure of amorphous silicon monoxide (SiO), *J. Non Cryst. Solids*, 320(2003), No. 1-3, p. 255.

[34] J.H. Kim, C.M. Park, H. Kim, Y.J. Kim, and H.J. Sohn, Electrochemical behavior of SiO anode for Li secondary batteries, *J. Electroanal. Chem.*, 661(2011), No. 1, p. 245.

[35] A. Hirata, S. Kohara, T. Asada, M. Arao, C. Yogi, H. Imai, Y.W. Tan, T. Fujita, and M.W. Chen, Atomic-scale disproportionation in amorphous silicon monoxide, *Nat. Commun.*, 7(2016), art. No. 11591.

[36] Y. Yao, J.J. Zhang, L.G. Xue, T. Huang, and A.S. Yu, Carbon-coated SiO_2 nanoparticles as anode material for lithium ion batteries, *J. Power Sources*, 196(2011), No. 23, p. 10240.

[37] B.K. Guo, J. Shu, Z.X. Wang, H. Yang, L.H. Shi, Y.N. Liu, and L.Q. Chen, Electrochemical reduction of nano-SiO_2 in hard carbon as anode material for lithium ion batteries, *Electrochem. Commun.*, 10(2008), No. 12, p. 1876.

[38] Q. Sun, B. Zhang, and Z.W. Fu, Lithium electrochemistry of SiO_2 thin film electrode for lithium-ion batteries, *Appl. Surf. Sci.*, 254(2008), No. 13, p. 3774.

[39] T. Kim, S. Park, and S.M. Oh, Solid-state NMR and electrochemical dilatometry study on Li^+ uptake/extraction mechanism in SiO electrode, *J. Electrochem. Soc.*, 154(2007), No. 12, art. No. A1112.

[40] Y. Yamada, Y. Iriyama, T. Abe, and Z. Ogumi, Kinetics of electrochemical insertion and extraction of lithium ion at SiO, *J. Electrochem. Soc.*, 157(2010), No. 1, art. No. A26.

[41] M. Yamada, A. Inaba, A. Ueda, K. Matsumoto, T. Iwasaki, and T. Ohzuku, Reaction mechanism of "SiO"-carbon composite-negative electrode for high-capacity lithium-ion batteries, *J. Electrochem. Soc.*, 159(2012), No. 10, p. A1630.

[42] H. Jung, B.C. Yeo, K.R. Lee, and S.S. Han, Atomistics of the lithiation of oxidized silicon (SiO_x) nanowires in reactive molecular dynamics simulations, *Phys. Chem. Chem. Phys.*, 18(2016), No. 47, p. 32078.

[43] H. Yamamura, K. Nobuhara, S. Nakanishi, H. Iba, and S. Okada, Investigation of the irreversible reaction mechanism and the reactive trigger on SiO anode material for lithium-ion battery, *J. Ceram. Soc. Jpn.*, 119(2011), No. 1395, p. 855.

[44] B.C. Yu, Y. Hwa, J.H. Kim, and H.J. Sohn, A new approach to synthesis of porous SiO_x anode for Li-ion batteries via chemical etching of Si crystallites, *Electrochim. Acta*, 117(2014), p. 426.

[45] B.C. Yu, Y. Hwa, C.M. Park, and H.J. Sohn, Reaction mechanism and enhancement of cyclability of SiO anodes by surface etching with NaOH for Li-ion batteries, *J. Mater. Chem. A*, 1(2013), No. 15, art. No. 4820.

[46] M. Miyachi, H. Yamamoto, H. Kawai, T. Ohta, and M. Shirakata, Analysis of SiO anodes for lithium-ion batteries, *J. Electrochem. Soc.*, 152(2005), No. 10, art. No. A2089.

[47] A. Veluchamy, C.H. Doh, D.H. Kim, J.H. Lee, D.J. Lee, K.H. Ha, H.M. Shin, B.S. Jin, H.S. Kim, S.I. Moon, and C.W. Park, Improvement of cycle behaviour of SiO/C anode composite by thermochemically generated Li_4SiO_4 inert phase for lithium batteries, *J. Power Sources*, 188(2009), No. 2, p. 574.

[48] X.L. Yang, Z.Y. Wen, X.X. Xu, B. Lin, and S.H. Huang, Nanosized silicon-based composite derived by *in situ* mechanochemical reduction for lithium ion batteries, *J. Power Sources*, 164(2007), No. 2, p. 880.

[49] T. Chen, J. Wu, Q.L. Zhang, and X. Su, Recent advancement of SiO_x based anodes for lithium-ion batteries, *J. Power Sources*, 363(2017), p. 126.

[50] Z.H. Liu, Q. Yu, Y.L. Zhao, R.H. He, M. Xu, S.H. Feng, S.D. Li, L. Zhou, and L.Q. Mai, Silicon oxides: A promising family of anode materials for lithium-ion batteries, *Chem. Soc. Rev.*, 48(2019), No. 1, p. 285.

[51] T. Wang, X.T. Guo, H.Y. Duan, C.Y. Chen, and H. Pang, SiO-based ($0 < x \leq 2$) composites for lithium-ion batteries, *Chin. Chem. Lett.*, 31(2020), No. 3, p. 654.

[52] Y. Hwa, C.M. Park, and H.J. Sohn, Modified SiO as a high performance anode for Li-ion batteries, *J. Power Sources*, 222(2013), p. 129.

[53] J.K. Lee, W.Y. Yoon, and B.K. Kim, Kinetics of reaction products of silicon monoxide with controlled amount of Li-ion insertion at various current densities for Li-ion batteries, *J. Electrochem. Soc.*, 161(2014), No. 6, p. A927.

[54] W.S. Chang, C.M. Park, J.H. Kim, Y.U. Kim, G. Jeong, and H.J. Sohn, Quartz (SiO_2): A new energy storage anode material for Li-ion batteries, *Energy Environ. Sci.*, 5(2012), No. 5, art. No. 6895.

[55] K. Yasuda, Y. Kashitani, S. Kizaki, K. Takeshita, T. Fujita, and S. Shimosaki, Thermodynamic analysis and effect of crystallinity for silicon monoxide negative electrode for lithium ion batteries, *J. Power Sources*, 329(2016), p. 462.

[56] M. Yamada, A. Ueda, K. Matsumoto, and T. Ohzuku, Silicon-based negative electrode for high-capacity lithium-ion batteries: "SiO"-carbon composite, *J. Electrochem. Soc.*, 158(2011), No. 4, art. No. A417.

[57] T. Tashiro, M. Dougakiuchi, and M. Kambara, Instantaneous formation of SiO_x nanocomposite for high capacity lithium ion batteries by enhanced disproportionation reaction during plasma spray physical vapor deposition, *Sci. Technol. Adv. Mater.*, 17(2016), No. 1, p. 744.

[58] Z.H. Liu, D.D. Guan, Q. Yu, L. Xu, Z.C. Zhuang, T. Zhu, D.Y. Zhao, L. Zhou, and L.Q. Mai, Monodisperse and homogeneous SiO_x/C microspheres: A promising high-capacity and durable anode material for lithium-ion batteries, *Energy Storage Mater.*, 13(2018), p. 112.

[59] C.F. Guo, D.L. Wang, T.F. Liu, J.S. Zhu, and X.S. Lang, A three dimensional SiO_x/C@RGO nanocomposite as a high energy anode material for lithium-ion batteries, *J. Mater. Chem. A*, 2(2014), No. 10, p. 3521.

[60] W.J. Wu, J. Shi, Y.H. Liang, F. Liu, Y. Peng, and H.B. Yang, A low-cost and advanced SiO_x–C composite with hierarchical structure as an anode material for lithium-ion batteries, *Phys. Chem. Chem. Phys.*, 17(2015), No. 20, p. 13451.

[61] M.S. Park, E. Park, J. Lee, G. Jeong, K.J. Kim, J.H. Kim, Y.J. Kim, and H. Kim, Hydrogen silsequioxane-derived Si/SiO_x nanospheres for high-capacity lithium storage materials, *ACS Appl. Mater. Interfaces*, 6(2014), No. 12, p. 9608.

[62] Y.D. Cao, J.C. Bennett, R.A. Dunlap, and M.N. Obrovac, A simple synthesis route for high-capacity SiO_x anode materials with tunable oxygen content for lithium-ion batteries, *Chem. Mater.*, 30(2018), No. 21, p. 7418.

[63] S.S. Suh, W.Y. Yoon, D.H. Kim, S.U. Kwon, J.H. Kim, Y.U. Kim, C.U. Jeong, Y.Y. Chan, S.H. Kang, and J.K. Lee, Electrochemical behavior of SiO_x anodes with variation of oxygen ratio for Li-ion batteries, *Electrochim. Acta*, 148(2014), p. 111.

[64] Y.J. Chen, J.B. Li, and J.H. Dai, Si and SiO_x nanostructures formed via thermal evaporation, *Chem. Phys. Lett.*, 344(2001), No. 5-6, p. 450.

[65] L. Shi, W.K. Wang, A.B. Wang, K.G. Yuan, Z.Q. Jin, and Y.S. Yang, Scalable synthesis of core-shell structured SiO_x/nitrogen-doped carbon composite as a high-performance anode material for lithium-ion batteries, *J. Power Sources*, 318(2016), p. 184.

[66] F.T. Ferguson and J.A. Nuth, Vapor pressure and evaporation coefficient of silicon monoxide over a mixture of silicon and silica, *J. Chem. Eng. Data*, 57(2012), No. 3, p. 721.

[67] M.K. Kim, B.Y. Jang, J.S. Lee, J.S. Kim, and S. Nahm, Microstructures and electrochemical performances of nano-sized SiO_x ($1.18 \leq x \leq 1.83$) as an anode material for a lithium(Li)-ion battery, *J. Power Sources*, 244(2013), p. 115.

[68] W.Y. Chen, R.V. Salvatierra, M.Q. Ren, J.H. Chen, M.G. Stanford, and J.M. Tour, Laser-induced silicon oxide for anode-free lithium metal batteries, *Adv. Mater.*, 32(2020), No.

33, art. No. 2002850.
[69] Y.X. Liu, J.J. Ruan, F. Liu, Y.M. Fan, and P. Wang, Synthesis of SiO_x/C composite with dual interface as Li-ion battery anode material, *J. Alloys Compd.*, 802(2019), p. 704.
[70] T. Xu, Q. Wang, J. Zhang, X.H. Xie, and B.J. Xia, Green synthesis of dual carbon conductive network-encapsulated hollow SiO_x spheres for superior lithium-ion batteries, *ACS Appl. Mater. Interfaces*, 11(2019), No. 22, p. 19959.
[71] P.P. Lü, H.L. Zhao, C.H. Gao, Z.H. Du, J. Wang, and X. Liu, SiO_x–C dual-phase glass for lithium ion battery anode with high capacity and stable cycling performance, *J. Power Sources*, 274(2015), p. 542.
[72] P.P. Lü, H.L. Zhao, C.H. Gao, T.H. Zhang, and X. Liu, Highly efficient and scalable synthesis of SiO_x/C composite with core-shell nanostructure as high-performance anode material for lithium ion batteries, *Electrochim. Acta*, 152(2015), p. 345.
[73] Z.L. Li, H.L. Zhao, P.P. Lü, Z.J. Zhang, Y. Zhang, Z.H. Du, Y.Q. Teng, L.N. Zhao, and Z.M. Zhu, Watermelon-like structured SiO_x–TiO_2@C nanocomposite as a high-performance lithium-ion battery anode, *Adv. Funct. Mater.*, 28(2018), No. 31, art. No. 1605711.
[74] Z.L. Li, H.L. Zhao, J. Wang, T.H. Zhang, B.Y. Fu, Z.J. Zhang, and X. Tao, Rational structure design to realize high-performance SiO_x@C anode material for lithium ion batteries, *Nano Res.*, 13(2020), No. 2, p. 527.
[75] J. Li and J.G. Huang, A nanofibrous polypyrrole/silicon composite derived from cellulose substance as the anode material for lithium-ion batteries, *Chem. Commun.*, 51(2015), No. 78, p. 14590.
[76] W. Liu, J.Z. Wang, J.T. Wang, X.Z. Guo, and H. Yang, Three-dimensional nitrogen-doped carbon coated hierarchically porous silicon composite as lithium-ion battery anode, *J. Alloys Compd.*, 874(2021), art. No. 159921.
[77] M.Y. Wang, D.L. Jia, J. Li, and J.G. Huang, Nanofibrous silicon/carbon composite sheet derived from cellulose substance as free-standing lithium-ion battery anodes, *RSC Adv.*, 4(2014), No. 64, p. 33981.
[78] D. Liu, C.R. Chen, Y.Y. Hu, J. Wu, D. Zheng, Z.Z. Xie, G.W. Wang, D.Y. Qu, J.S. Li, and D.Y. Qu, Reduced graphene-oxide/highly ordered mesoporous SiO_x hybrid material as an anode material for lithium ion batteries, *Electrochim. Acta*, 273(2018), p. 26.
[79] J.Y. Zhang, P.P. Ma, Z.L. Hou, X.M. Zhang, and C.B. Li, One-step synthesis of SiO_x@graphene composite material by a hydrothermal method for lithium-ion battery anodes, *Energy Fuels*, 34(2020), No. 3, p. 3895.
[80] J.Y. Zhang, Z.L. Hou, X.M. Zhang, L.C. Zhang, and C.B. Li, Delicate construction of Si@SiO_x composite materials by microwave hydrothermal for lithium-ion battery anodes, *Ionics*, 26(2020), No. 1, p. 69.
[81] Y.R. Ren and M.Q. Li, Facile synthesis of SiO_x@C composite nanorods as anodes for lithium ion batteries with excellent electrochemical performance, *J. Power Sources*, 306(2016), p. 459.
[82] C.H. Gao, H.L. Zhao, P.P. Lü, C.M. Wang, J. Wang, T.H. Zhang, and Q. Xia, Superior cycling performance of SiO_x/C composite with arrayed mesoporous architecture as anode material for lithium-ion batteries, *J. Electrochem. Soc.*, 161(2014), No. 14, p. A2216.
[83] Y.R. Ren, X.M. Wu, and M.Q. Li, Highly stable SiO_x/multi-wall carbon nanotube/N-doped carbon composite as anodes for lithium-ion batteries, *Electrochim. Acta*, 206(2016), p. 328.
[84] J. Wang, H.L. Zhao, J.C. He, C.M. Wang, and J. Wang, Nano-sized SiO_x/C composite anode for lithium ion batteries, *J. Power Sources*, 196(2011), No. 10, p. 4811.
[85] Z.L. Li, N.N. Yao, H.L. Zhao, Z. Yang, B.Y. Fu, and J. Wang, Communication—self-template fabrication of porous Si/SiO_x/C anode material for lithium-ion batteries, *J. Electrochem. Soc.*, 167(2020), No. 2, art. No. 020555.
[86] J. Hwang, K. Kim, W.S. Jung, H. Choi, and J.H. Kim, Facile and scalable synthesis of SiO_x materials for Li-ion negative electrodes, *J. Power Sources*, 436(2019), art. No. 226883.
[87] Y.D. Cao, R.A. Dunlap, and M.N. Obrovac, Electrochemistry and thermal behavior of SiO_x made by reactive gas milling, *J. Electrochem. Soc.*, 167(2020), No. 11, art. No. 110501.
[88] D.H. Xu, W.Y. Chen, Y.L. Luo, H.S. Wei, C.J. Yang, X. Cai, Y.P. Fang, and X.Y. Yu, Amorphous TiO_2 layer on silicon monoxide nanoparticles as stable and scalable core-shell anode materials for high performance lithium ion batteries, *Appl. Surf. Sci.*, 479(2019), p. 980.
[89] Z.X. Xiao, C.H. Yu, X.Q. Lin, X. Chen, C.X. Zhang, H.R. Jiang, R.F. Zhang, and F. Wei, TiO_2 as a multifunction coating layer to enhance the electrochemical performance of SiO_x@TiO_2@C composite as anode material, *Nano Energy*, 77(2020), art. No. 105082.
[90] Z.Y. Wang, N. Yang, L. Ren, X.M. Wang, and X. Zhang, Core-shell structured SiO_x@C with controllable mesopores as anode materials for lithium-ion batteries, *Microporous Mesoporous Mater.*, 307(2020), art. No. 110480.
[91] L. Liu, X.X. Li, G. He, G.Q. Zhang, G.J. Su, and C.H. Fang, SiO@C/TiO_2 nanospheres with dual stabilized architecture as anode material for high-performance Li-ion battery, *J. Alloys Compd.*, 836(2020), art. No. 155407.
[92] J. Bae, D.S. Kim, H. Yoo, E. Park, Y.G. Lim, M.S. Park, Y.J. Kim, and H. Kim, High-performance Si/SiO_x nanosphere anode material by multipurpose interfacial engineering with black TiO_{2-x}, *ACS Appl. Mater. Interfaces*, 8(2016), No. 7, p. 4541.
[93] J.G. Guo, W. Zhai, Q. Sun, Q. Ai, J. Li, J. Cheng, L.N. Dai, and L.J. Ci, Facilely tunable core-shell Si@SiO_x nanostructures prepared in aqueous solution for lithium ion battery anode, *Electrochim. Acta*, 342(2020), art. No. 136068.
[94] F. Dou, Y.H. Weng, G.R. Chen, L.Y. Shi, H.J. Liu, and D.S. Zhang, Volume expansion restriction effects of thick TiO_2/C hybrid coatings on micro-sized SiO_x anode materials, *Chem. Eng. J.*, 387(2020), art. No. 124106.
[95] Z.G. Teng, X.D. Su, Y.Y. Zheng, J. Sun, G.T. Chen, C.C. Tian, J.D. Wang, H. Li, Y.N. Zhao, and G.M. Lu, Mesoporous silica hollow spheres with ordered radial mesochannels by a spontaneous self-transformation approach, *Chem. Mater.*, 25(2013), No. 1, p. 98.
[96] J.I. Lee and S. Park, High-performance porous silicon monoxide anodes synthesized via metal-assisted chemical etching, *Nano Energy*, 2(2013), No. 1, p. 146.
[97] Y.Y. Zhang, G.W. Hu, Q. Yu, Z.H. Liu, C. Yu, L.S. Wu, L. Zhou, and L.Q. Mai, Polydopamine sacrificial layer mediated SiO_x/C@C yolk@shell structure for durable lithium storage, *Mater. Chem. Front.*, 4(2020), No. 6, p. 1656.
[98] Z.H. Liu, Y.L. Zhao, R.H. He, W. Luo, J.S. Meng, Q. Yu, D.Y. Zhao, L. Zhou, and L.Q. Mai, Yolk@shell SiO_x/C microspheres with semi-graphitic carbon coating on the exterior and interior surfaces for durable lithium storage, *Energy Storage Mater.*, 19(2019), p. 299.
[99] D.L. He, P. Li, W. Wang, Q. Wan, J. Zhang, K. Xi, X.M. Ma, Z.W. Liu, L. Zhang, and X.H. Qu, Collaborative design of hollow nanocubes, *in situ* cross-linked binder, and amorphous void@SiO_x@C as a three-pronged strategy for ultrastable lithium storage, *Small*, 16(2020), No. 5, art. No. 1905736.
[100] J.Y. Zhang, X.M. Zhang, C.Q. Zhang, Z. Liu, J. Zheng, Y.H. Zuo, C.L. Xue, C.B. Li, and B.W. Cheng, Facile and efficient synthesis of a microsized SiO_x/C core–shell composite as anode material for lithium ion batteries, *Energy Fuels*, 31(2017), No. 8, p. 8758.
[101] S.J. Lee, H.J. Kim, T.H. Hwang, S. Choi, S.H. Park, E. Deniz,

D.S. Jung, and J.W. Choi, Delicate structural control of Si–Si-O_x–C composite via high-speed spray pyrolysis for Li-ion battery anodes, *Nano Lett.*, 17(2017), No. 3, p. 1870.

[102] R. Wang, J. Wang, S. Chen, C.L. Jiang, W. Bao, Y.F. Su, G.Q. Tan, and F. Wu, Toward mechanically stable silicon-based anodes using Si/SiO_x@C hierarchical structures with well-controlled internal buffer voids, *ACS Appl. Mater. Interfaces*, 10(2018), No. 48, p. 41422.

[103] G. Li, J.Y. Li, F.S. Yue, Q. Xu, T.T. Zuo, Y.X. Yin, and Y.G. Guo, Reducing the volume deformation of high capacity SiO_x/G/C anode toward industrial application in high energy density lithium-ion batteries, *Nano Energy*, 60(2019), p. 485.

[104] X.L. He, W. Zhao, D.D. Li, P.J. Cai, Q.C. Zhuang, and Z.C. Ju, A long-cycle and high-rate Si/SiO_x/nitrogen-doped carbon composite as an anode material for lithium-ion batteries, *New J. Chem.*, 43(2019), No. 46, p. 18220.

[105] X. Gao, X.C. Sun, J.S. Liu, N. Gao, and H.D. Li, A carbon-based anode combining with SiO_x and nanodiamond for high performance lithium ion battery, *J. Energy Storage*, 25(2019), art. No. 100901.

[106] D. Liu, K. Fang, X.H. You, H.L. Tang, Z.Z. Xie, J.S. Li, X. Li, and D.Y. Qu, Formation of thin layer graphite wrapped meso-porous SiO_x and its lithium storage application, *Ceram. Int.*, 45(2019), No. 18, p. 24707.

[107] Z.X. Xiao, C.H. Yu, X.Q. Lin, X. Chen, C.X. Zhang, and F. Wei, Uniform coating of nano-carbon layer on SiO_x in aggregated fluidized bed as high-performance anode material, *Carbon*, 149(2019), p. 462.

[108] M.S. Han and J. Yu, Subnanoscopically and homogeneously dispersed SiO_x/C composite spheres for high-performance lithium ion battery anodes, *J. Power Sources*, 414(2019), p. 435.

[109] J.Y. Zhang, X.M. Zhang, Z.L. Hou, L.C. Zhang, and C.B. Li, Uniform SiO_x/graphene composite materials for lithium ion battery anodes, *J. Alloys Compd.*, 809(2019), art. No. 151798.

[110] L.Y. Chen, J. Zheng, S.Y. Lin, S. Khan, J.L. Huang, S.H. Liu, Z.R. Chen, D.C. Wu, and R.W. Fu, Synthesis of SiO_x/C composite nanosheets as high-rate and stable anode materials for lithium-ion batteries, *ACS Appl. Energy Mater.*, 3(2020), No. 4, p. 3562.

[111] J.L. Cui, H.B. Zhang, Y.Y. Liu, S.H. Li, W.X. He, J.L. Hu, and J.C. Sun, Facile, economical and environment-friendly synthesis process of porous N-doped carbon/SiO_x composite from rice husks as high-property anode for Li-ion batteries, *Electrochim. Acta*, 334(2020), art. No. 135619.

[112] M.S. Han, Y.B. Mu, F. Yuan, J.B. Liang, T. Jiang, X.D. Bai, and J. Yu, Vertical graphene growth on uniformly dispersed sub-nanoscale SiO_x/N-doped carbon composite microspheres with a 3D conductive network and an ultra-low volume deformation for fast and stable lithium-ion storage, *J. Mater. Chem. A*, 8(2020), No. 7, p. 3822.

[113] W.Y. Chen, D.H. Xu, S.J. Kuang, Z.Q. Wu, H. Hu, M.T. Zheng, and X.Y. Yu, Hierarchically porous SiO_x/C and carbon materials from one biomass waste precursor toward high-performance lithium/sodium storage, *J. Power Sources*, 489(2021), art. No. 229459.

[114] W.Y. Chen, H.F. Liu, S.J. Kuang, H.Y. Huang, T. Tang, M.T. Zheng, Y.P. Fang, and X.Y. Yu, *In-situ* low-temperature strategy from waste sugarcane leaves towards micro/meso-porous carbon network embedded nano Si–SiO_x@C boosting high performances for lithium-ion batteries, *Carbon*, 179(2021), p. 377.

[115] J.W. Ge, Q.T. Tang, H.L. Shen, F. Zhou, H.B. Zhou, W.Y. Yang, J. Hong, B.B. Xu, and J. Saddique, Controllable preparation of disproportionated SiO_x/C sheets with 3D network as high-performance anode materials of lithium ion battery, *Appl. Surf. Sci.*, 552(2021), art. No. 149446.

[116] M. Xia, Y.R. Li, Y.F. Wu, H.B. Zhang, J.K. Yang, N. Zhou, Z. Zhou, and X. Xiong, Improving the electrochemical properties of a SiO@C/graphite composite anode for high-energy lithium-ion batteries by adding lithium fluoride, *Appl. Surf. Sci.*, 480(2019), p. 410.

[117] M.Q. Li, Y. Zeng, Y.R. Ren, C.M. Zeng, J.W. Gu, X.F. Feng, and H.Y. He, Fabrication and lithium storage performance of sugar apple-shaped SiO_x@C nanocomposite spheres, *J. Power Sources*, 288(2015), p. 53.

[118] C.H. Gao, H.L. Zhao, J. Wang, J. Wang, C.L. Yan, and H.Q. Yin, Self-assembly of hierarchical silicon suboxide nanoparticles encapsulated in nitrogen-doped carbon as high performance anode material for lithium-ion batteries, *J. Electrochem. Soc.*, 166(2019), No. 4, p. A574.

[119] W.L. Guo, X. Yan, F. Hou, L. Wen, Y.J. Dai, D.M. Yang, X.T. Jiang, J. Liu, J. Liang, and S.X. Dou, Flexible and free-standing SiO_x/CNT composite films for high capacity and durable lithium ion batteries, *Carbon*, 152(2019), p. 888.

[120] X.Y. Wang, Z.Y. Wen, Y. Liu, and X.W. Wu, A novel composite containing nanosized silicon and tin as anode material for lithium ion batteries, *Electrochim. Acta*, 54(2009), No. 20, p. 4662.

[121] X.Y. Wang, Z.Y. Wen, Y. Liu, X.G. Xu, and J. Lin, Preparation and characterization of a new nanosized silicon–nickel–graphite composite as anode material for lithium ion batteries, *J. Power Sources*, 189(2009), No. 1, p. 121.

[122] J.H. Yom, J.K. Lee, and W.Y. Yoon, Improved electrochemical behavior of W-coated SiO–graphite composite anode in lithium-ion secondary battery, *J. Appl. Electrochem.*, 45(2015), No. 5, p. 397.

[123] J.K. Lee, J.H. Lee, B.K. Kim, and W.Y. Yoon, Electrochemical characteristics of diamond-like carbon/Cr double-layer coating on silicon monoxide-graphite composite anode for Li-ion batteries, *Electrochim. Acta*, 127(2014), p. 1.

[124] J.Z. Zhang, J. Zhang, T.Z. Bao, X.H. Xie, and B.J. Xia, Electrochemical and stress characteristics of SiO/Cu/expanded graphite composite as anodes for lithium ion batteries, *J. Power Sources*, 348(2017), p. 16.

[125] N. Zhou, Y.F. Wu, Q. Zhou, Y.R. Li, S.H. Liu, H.B. Zhang, Z. Zhou, and M. Xia, Enhanced cycling performance and rate capacity of SiO anode material by compositing with monoclinic TiO_2 (B), *Appl. Surf. Sci.*, 486(2019), p. 292.

[126] G. Jeong, J.H. Kim, Y.U. Kim, and Y.J. Kim, Multifunctional TiO_2 coating for a SiO anode in Li-ion batteries, *J. Mater. Chem.*, 22(2012), No. 16, art. No. 7999.

[127] M.J. Zhou, M.L. Gordin, S.R. Chen, T. Xu, J.X. Song, D.P. Lü, and D.H. Wang, Enhanced performance of SiO/Fe_2O_3 composite as an anode for rechargeable Li-ion batteries, *Electrochem. Commun.*, 28(2013), p. 79.

[128] F. Cheng, G.J. Wang, Z.X. Sun, Y. Yu, F. Huang, C.L. Gong, H. Liu, G.W. Zheng, C.Q. Qin, and S. Wen, Carbon-coated SiO/ZrO_2 composites as anode materials for lithium-ion batteries, *Ceram. Int.*, 43(2017), No. 5, p. 4309.

[129] Z.Q. Gu, W.L. Li, Y.X. Chen, X.H. Xia, and H.B. Liu, Synthesis of the microspherical structure of ternary SiO_x@SnO_2@C by a hydrothermal method as the anode for high-performance lithium-ion batteries, *Sustain. Energy Fuels*, 4(2020), No. 5, p. 2333.

[130] B. Liu, A. Abouimrane, Y. Ren, M. Balasubramanian, D.P. Wang, Z.Z. Fang, and K. Amine, New anode material based on SiO–$Sn_xCo_yC_z$ for lithium batteries, *Chem. Mater.*, 24(2012), No. 24, p. 4653.

[131] B. Liu, A. Abouimrane, D.E. Brown, X.F. Zhang, Y. Ren, Z.Z. Fang, and K. Amine, Mechanically alloyed composite anode materials based on SiO–$Sn_xFe_yC_z$ for Li-ion batteries, *J. Mater. Chem. A*, 1(2013), No. 13, art. No. 4376.

[132] L.Y. Beaulieu, K.W. Eberman, R.L. Turner, L.J. Krause, and J.R. Dahn, Colossal reversible volume changes in lithium al-

loys, *Electrochem. Solid-State Lett.*, 4(2001), No. 9, art. No. A137.
[133] Z.H. Lin, J.H. Li, Q.M. Huang, K. Xu, W.Z. Fan, L. Yu, Q.B. Xia, and W.S. Li, Insights into the interfacial instability between carbon-coated SiO anode and electrolyte in lithium-ion batteries, *J. Phys. Chem. C*, 123(2019), No. 20, p. 12902.
[134] T. Jaumann, J. Balach, U. Langklotz, V. Sauchuk, M. Fritsch, A. Michaelis, V. Teltevskij, D. Mikhailova, S. Oswald, M. Klose, G. Stephani, R. Hauser, J. Eckert, and L. Giebeler, Lifetime vs. rate capability: Understanding the role of FEC and VC in high-energy Li-ion batteries with nano-silicon anodes, *Energy Storage Mater.*, 6(2017), p. 26.
[135] Z.X. Xu, J. Yang, H.P. Li, Y.N. Nuli, and J.L. Wang, Electrolytes for advanced lithium ion batteries using silicon-based anodes, *J. Mater. Chem. A*, 7(2019), No. 16, p. 9432.
[136] Y.H. Sun, L. Fan, W.Y. Li, Y. Pang, J. Yang, C.X. Wang, and Y.Y. Xia, SiO_x and carbon double-layer coated Si nanorods as anode materials for lithium-ion batteries, *RSC Adv.*, 6(2016), No. 103, p. 101008.
[137] Y.H. Liu, M. Okano, T. Mukai, K. Inoue, M. Yanagida, and T. Sakai, Improvement of thermal stability and safety of lithium ion battery using SiO anode material, *J. Power Sources*, 304(2016), p. 9.
[138] X. Huang and M.Q. Li, Multi-channel and porous SiO@N-doped C rods as anodes for high-performance lithium-ion batteries, *Appl. Surf. Sci.*, 439(2018), p. 336.
[139] L.B. Chen, K. Wang, X.H. Xie, and J.Y. Xie, Enhancing electrochemical performance of silicon film anode by vinylene carbonate electrolyte additive, *Electrochem. Solid-State Lett.*, 9(2006), No. 11, art. No. A512.
[140] N.S. Choi, K.H. Yew, K.Y. Lee, M. Sung, H. Kim, and S.S. Kim, Effect of fluoroethylene carbonate additive on interfacial properties of silicon thin-film electrode, *J. Power Sources*, 161(2006), No. 2, p. 1254.
[141] H. Nakai, T. Kubota, A. Kita, and A. Kawashima, Investigation of the solid electrolyte interphase formed by fluoroethylene carbonate on Si electrodes, *J. Electrochem. Soc.*, 158(2011), No. 7, p. A798.
[142] T. Jaumann, J. Balach, M. Klose, S. Oswald, U. Langklotz, A. Michaelis, J. Eckert, and L. Giebeler, SEI-component formation on sub 5 nm sized silicon nanoparticles in Li-ion batteries: The role of electrode preparation, FEC addition and binders, *Phys. Chem. Chem. Phys.*, 17(2015), No. 38, p. 24956.
[143] Y.Z. Yang, Z. Yang, Y.S. Xu, Z.L. Li, N.N. Yao, J. Wang, Z.H. Feng, K. Wang, J.Y. Xie, and H.L. Zhao, Synergistic effect of vinylene carbonate (VC) and $LiNO_3$ as functional additives on interphase modulation for high performance SiO anodes, *J. Power Sources*, 514(2021), art. No. 230595.
[144] J.Q. Shen, H.F. Chen, L. Yu, D.H. Huang, and Z.Y. Luo, 4, 5-difluoro-1, 3-dioxolan-2-one as an film forming additive on $LiNi_{0.8}Co_{0.15}Al_{0.05}O_2$/SiO@C full cells, *J. Electroanal. Chem.*, 834(2019), p. 1.
[145] K.W. Kim, J.G. Lee, H. Park, J. Kim, J.H. Ryu, Y.U. Kim, and S.M. Oh, Effect of lithium bis(oxalate)borate as an electrolyte additive on carbon-coated SiO negative electrode, *J. Korean Electrochem. Soc.*, 17(2014), No. 1, p. 49.
[146] J.W. Song, C.C. Nguyen, and S.W. Song, Stabilized cycling performance of silicon oxide anode in ionic liquid electrolyte for rechargeable lithium batteries, *RSC Adv.*, 2(2012), No. 5, art. No. 2003.
[147] M.W. Forney, M.J. Ganter, J.W. Staub, R.D. Ridgley, and B.J. Landi, Prelithiation of silicon-carbon nanotube anodes for lithium ion batteries by stabilized lithium metal powder (SLMP), *Nano Lett.*, 13(2013), No. 9, p. 4158.
[148] C.R. Jarvis, M.J. Lain, M.V. Yakovleva, and Y. Gao, A prelithiated carbon anode for lithium-ion battery applications, *J. Power Sources*, 162(2006), No. 2, p. 800.
[149] M. Marinaro, M. Weinberger, and M. Wohlfahrt-Mehrens, Toward pre-lithiatied high areal capacity silicon anodes for Lithium-ion batteries, *Electrochim. Acta*, 206(2016), p. 99.
[150] Q.R. Pan, P.J. Zuo, T.S. Mu, C.Y. Du, X.Q. Cheng, Y.L. Ma, Y.Z. Gao, and G.P. Yin, Improved electrochemical performance of micro-sized SiO-based composite anode by prelithiation of stabilized lithium metal powder, *J. Power Sources*, 347(2017), p. 170.
[151] H. Zhao, Y.B. Fu, M. Ling, Z. Jia, X.Y. Song, Z.H. Chen, J. Lu, K. Amine, and G. Liu, Conductive polymer binder-enabled SiO–$Sn_xCo_yC_z$ anode for high-energy lithium-ion batteries, *ACS Appl. Mater. Interfaces*, 8(2016), No. 21, p. 13373.
[152] T. Tabuchi, H. Yasuda, and M. Yamachi, Li-doping process for Li_xSiO-negative active material synthesized by chemical method for lithium-ion cells, *J. Power Sources*, 146(2005), No. 1-2, p. 507.
[153] G.W. Wang, F.F. Li, D. Liu, D. Zheng, Y. Luo, D.Y. Qu, T.Y. Ding, and D.Y. Qu, Chemical prelithiation of negative electrodes in ambient air for advanced lithium-ion batteries, *ACS Appl. Mater. Interfaces*, 11(2019), No. 9, p. 8699.
[154] Y.F. Shen, J.M. Zhang, Y.F. Pu, H. Wang, B. Wang, J.F. Qian, Y.L. Cao, F.P. Zhong, X.P. Ai, and H.X. Yang, Effective chemical prelithiation strategy for building a silicon/sulfur Li-ion battery, *ACS Energy Lett.*, 4(2019), No. 7, p. 1717.
[155] M.Y. Yan, G. Li, J. Zhang, Y.F. Tian, Y.X. Yin, C.J. Zhang, K.C. Jiang, Q. Xu, H.L. Li, and Y.G. Guo, Enabling SiO_x/C anode with high initial coulombic efficiency through a chemical pre-lithiation strategy for high-energy-density lithium-ion batteries, *ACS Appl. Mater. Interfaces*, 12(2020), No. 24, p. 27202.
[156] X.J. Feng, J. Yang, X.L. Yu, J.L. Wang, and Y.N. Nuli, Low-cost SiO-based anode using green binders for lithium ion batteries, *J. Solid State Electrochem.*, 17(2013), No. 9, p. 2461.
[157] T.L. Kulova and A.M. Skundin, Elimination of irreversible capacity of amorphous silicon: Direct contact of the silicon and lithium metal, *Russ. J. Electrochem.*, 46(2010), No. 4, p. 470.
[158] Q.H. Meng, G. Li, J.P. Yue, Q. Xu, Y.X. Yin, and Y.G. Guo, High-performance lithiated SiO_x anode obtained by a controllable and efficient prelithiation strategy, *ACS Appl. Mater. Interfaces*, 11(2019), No. 35, p. 32062.
[159] H.J. Kim, S. Choi, S.J. Lee, M.W. Seo, J.G. Lee, E. Deniz, Y.J. Lee, E.K. Kim, and J.W. Choi, Controlled prelithiation of silicon monoxide for high performance lithium-ion rechargeable full cells, *Nano Lett.*, 16(2016), No. 1, p. 282.
[160] M. Noh and J. Cho, Role of Li_6CoO_4 cathode additive in Li-ion cells containing low coulombic efficiency anode material, *J. Electrochem. Soc.*, 159(2012), No. 8, p. A1329.
[161] K. Park, B.C. Yu, and J.B. Goodenough, Li_3N as a cathode additive for high-energy-density lithium-ion batteries, *Adv. Energy Mater.*, 6(2016), No. 10, art. No. 1502534.
[162] Y.T. Bie, J. Yang, J.L. Wang, J.J. Zhou, and Y.N. Nuli, Li_2O_2 as a cathode additive for the initial anode irreversibility compensation in lithium-ion batteries, *Chem. Commun.*, 53(2017), No. 59, p. 8324.
[163] G. Jeong, Y.U. Kim, S.A. Krachkovskiy, and C.K. Lee, A nanostructured $SiAl_{0.2}O$ anode material for lithium batteries, *Chem. Mater.*, 22(2010), No. 19, p. 5570.
[164] J. Nam, E. Kim, R. K, Y. Kim, and T.H. Kim, A conductive self healing polymeric binder using hydrogen bonding for Si anodes in lithium ion batteries, *Sci. Rep.*, 10(2020), art. No. 14966.
[165] C. Wang, H. Wu, Z. Chen, M.T. McDowell, Y. Cui, and Z. Bao, Self-healing chemistry enables the stable operation of silicon microparticle anodes for high-energy lithium-ion batteries, *Nat. Chem.*, 5(2013), No. 12, p. 1042.
[166] U.S. Vogl, P.K. Das, A.Z. Weber, M. Winter, R. Kostecki, and S.F. Lux, Mechanism of interactions between CMC binder and

Si single crystal facets, *Langmuir*, 30(2014), No. 34, p. 10299.
[167] J. Yoon, D.X. Oh, C. Jo, J. Lee, and D.S. Hwang, Improvement of desolvation and resilience of alginate binders for Si-based anodes in a lithium ion battery by calcium-mediated cross-linking, *Phys. Chem. Chem. Phys.*, 16(2014), No. 46, p. 25628.
[168] D. Chen, R. Yi, S.R. Chen, T. Xu, M.L. Gordin, and D.H. Wang, Facile synthesis of graphene-silicon nanocomposites with an advanced binder for high-performance lithium-ion battery anodes, *Solid State Ionics*, 254(2014), p. 65.
[169] R. Kuruba, M.K. Datta, K. Damodaran, P.H. Jampani, B. Gattu, P.P. Patel, P.M. Shanthi, S. Damle, and P.N. Kumta, Guar gum: Structural and electrochemical characterization of natural polymer based binder for silicon-carbon composite rechargeable Li-ion battery anodes, *J. Power Sources*, 298(2015), p. 331.
[170] L. Yue, L.Z. Zhang, and H.X. Zhong, Carboxymethyl chitosan: A new water soluble binder for Si anode of Li-ion batteries, *J. Power Sources*, 247(2014), p. 327.
[171] Y.K. Jeong, T.W. Kwon, I. Lee, T.S. Kim, A. Coskun, and J.W. Choi, Hyperbranched β-cyclodextrin polymer as an effective multidimensional binder for silicon anodes in lithium rechargeable batteries, *Nano Lett.*, 14(2014), No. 2, p. 864.
[172] S. Komaba, K. Shimomura, N. Yabuuchi, T. Ozeki, H. Yui, and K. Konno, Study on polymer binders for high-capacity SiO negative electrode of Li-ion batteries, *J. Phys. Chem. C*, 115(2011), No. 27, p. 13487.
[173] A. Magasinski, B. Zdyrko, I. Kovalenko, B. Hertzberg, R. Burtovyy, C.F. Huebner, T.F. Fuller, I. Luzinov, and G. Yushin, Toward efficient binders for Li-ion battery Si-based anodes: Polyacrylic acid, *ACS Appl. Mater. Interfaces*, 2(2010), No. 11, p. 3004.
[174] Z. Liu, S.J. Han, C. Xu, Y.W. Luo, N. Peng, C.Y. Qin, M.J. Zhou, W.Q. Wang, L.W. Chen, and S. Okada, *In situ* cross-linked PVA–PEI polymer binder for long-cycle silicon anodes in Li-ion batteries, *RSC Adv.*, 6(2016), No. 72, p. 68371.
[175] S. Huang, J.G. Ren, R. Liu, M. Yue, Y.Y. Huang, and G.H. Yuan, The progress of novel binder as a non-ignorable part to improve the performance of Si-based anodes for Li-ion batteries, *Int. J. Energy Res.*, 42(2018), No. 3, p. 919.
[176] X.Y. Zhu, F. Zhang, L. Zhang, L.Y. Zhang, Y.Z. Song, T. Jiang, S. Sayed, C. Lu, X.G. Wang, J.Y. Sun, and Z.F. Liu, A highly stretchable cross-linked polyacrylamide hydrogel as an effective binder for silicon and sulfur electrodes toward durable lithium-ion storage, *Adv. Funct. Mater.*, 28(2018), No. 11, art. No. 1705015.
[177] L.X. Zhang, Z.H. Liu, G.L. Cui, and L.Q. Chen, Biomass-derived materials for electrochemical energy storages, *Prog. Polym. Sci.*, 43(2015), p. 136.
[178] Y. Cho, J. Kim, A. Elabd, S. Choi, K. Park, T.W. Kwon, J. Lee, K. Char, A. Coskun, and J.W. Choi, A pyrene–poly(acrylic acid)–polyrotaxane supramolecular binder network for high-performance silicon negative electrodes, *Adv. Mater.*, 31(2019), No. 51, art. No. 1905048.